Discovery of anti-fungal compounds from the immunobiome of North American bat species threatened by fungal infection with *Pseudogymnoascus destructans*

By
Jennifer Lynn Kolwich

A Thesis Submitted to
Saint Mary's University, Halifax, Nova Scotia
in Partial Fulfillment of the Requirements for
the Degree of Bachelor of Science with Honours in Chemistry

April 2019, Halifax, Nova Scotia

Approved: Dr. Clarissa Sit
Associate Professor,
Supervisor

Approved: Dr. Jason Masuda
Department Chair

Date: April 24, 2019

Discovery of anti-fungal compounds from the immunobiome of North American bat species threatened by fungal infection with *Pseudogymnoascus destructans*

by Jennifer Lynn Kolwich

ABSTRACT

With the spread of bat White-nose Syndrome decimating regional bat populations, finding a safe antifungal agent able to combat the causative agent *Pseudogymnoascus destructans* is a necessity. Upsetting the already fragile microbial balance on the skin of bats with, or at risk of developing, White-nose Syndrome is ill-advised. To avoid this, microbes that already reside on the skin of bats and in their hibernacula have been screened for anti-fungal activity.

Co-culturing cutaneous and environmental microbes against *Pseudogymnoascus destructans* and closely related species has yielded many potential candidates for antifungal bioactivity. The nature of the bioactivity was assessed by extracting the potentially antifungal compounds, screening them alone for bioactivity, and obtaining LC/MS profiles of all extracted compounds.

While five prime candidates were screened for activity, it was found that four were only able to produce significant inhibition when cocultured, indicating that their bioactivity is a result of resource competition or induction of antifungal compounds under the stress of co-culture conditions. The final strain shows innate antifungal properties based on the treatment of the *Pseudogymnoascus* fungi with compounds produced by the pure isolate strain. It shows increased bioactivity against *Pseudogymnoascus destructans*, specifically. The extracted compounds have been found to be stable for at least four weeks in solution without degrading and were able to maintain bioactivity for 8 weeks.

April 24, 2019

ACKNOWLEDGEMENTS

First, I would like to thank my supervisor, Dr. Clarissa Sit, for her support, guidance, and encouragement to seek out creative and novel solutions to difficult problems. Without her, I would not be as educated, nor as passionate about research (or bats, for that matter).

I would also like to thank the current Sit Research Group (Julie, Morgan, Kaitlyn, Brandon, Prashansa, Cassie, Kaleigh, and Abdurrahman) with special thanks to the Sit Bat Team members Lindsay and Iain, without whom I would have been far less productive and far more stressed!

Also, a special thanks to the Chemistry Department for this opportunity and their continued support, Alyssa Doué for dealing with my constant requests and questions, and Patricia Granados for her patience while training me on the LC/MS.

I would also like to acknowledge our collaborators Dr. Paul Faure from McMaster University, Hamilton, Ontario; Dr. Myron Smith from Carleton University, Ottawa, Ontario; and Dr. Hugh Broders from University of Waterloo, Waterloo, Ontario.

Finally, I would like to thank my family (especially my wonderful parents) and friends for helping me make it to this point and supporting me when I felt overwhelmed, stressed, or completely exhausted.

TABLE OF CONTENTS

List of Abbreviations:

WNS	White-nose Syndrome
Pd	*Pseudogymnoascus destructans*
ITS	Internally transcribed spacer
VOCs	Volatile organic compounds
RNA	Ribonucleic acid
Pb	*Pseudogymnoascus bhatti*
Pp	*Geomyces (Pseudogymnoascus) pannorum*
Pr	*Pseudogymnoascus roseus*
Pga	*Pseudogymnoascus*
R2A	Reasoner's 2A
YMA	Yeast malt agar
YMB	Yeast malt broth
dH_2O	Deionized water
ZOI	Zone of inhibition
HPLC	High-performance liquid chromatography
LC/MS/DAD	Liquid chromatography paired with mass spectrometry and a diode array detector

List of Tables:

List of Figures:

1. Introduction

1.1 Physiology and Anatomy of Chiropterans

Chiropterans, or bats, are diverse and unique organisms; bats are the second largest order of class Mammalia and the only mammalian order capable of self-sustained flight.[1] A behavioural adaptation characteristic of bats in colder climates is hibernation. In the winter, bats will enter a low metabolic state known as torpor for bouts spanning from a few days to a month.[1] In the state of torpor, bats will reduce their body temperature to match the ambient temperature of the hibernacula, as well as reducing their heart rate and breathing from 200-300 beats/min and 100-200 breaths/min, to 3-5 beats/min and 4-6 breaths/min, respectively.[1,2] To account for the extended period without food and water, bats will build up their fatty tissue before entering torpor to allow for them to be broken down by fatty acid oxidation. While in torpor, the bat's metabolism drops to nearly 1% of their euthermic states, requiring some functions to be sacrificed—such as immune, circulatory, and pulmonary-respiratory functions.[1]

Their patagium, or wing membrane, is possibly their most exceptional structural feature, both morphologically and functionally. The skin of the patagium is distinct from the skin of the rest of the body; it is highly folded and at least ten times thinner than the skin covering the rest of the body.[3] Composed of two epidermal layers encasing a vascularized connective tissue core, the patagium acts as a surface for passive gas exchange, but also evaporative water loss.[2,3] The sebaceous and apocrine glands on the wing provide a moisturising and waterproofing layer to the surface of the skin, but even still, up to 99% of the water loss in a hibernating bat occurs due to evaporative water loss. This layer is also thought to interact with the skin microbiome of bats by providing

nutrients to beneficial microbes, while acting as a barrier against harmful ones.[2] However, as evident by the recent outbreak of bat White-nose Syndrome in North America, this mechanism is not perfect.

1.2 White-Nose Syndrome and Pseudogymnoascus destructans

White-nose Syndrome (WNS) is a fungal infection that has decimated some North American bat populations. Since the first documented case in New York in 2006, WNS has spread to 33 states and 7 provinces (as of March 2019).[4–6] Some species have been classified as regionally endangered or extinct with population decreases from 90-100% in some counties.[4,5,7] WNS is characterized by the presence of a powdery white growth of fungus *Pseudogymnoascus destructans (Pd)* on the muzzle, ears and patagium of hibernating bats. [5,8,9]

This previously uncharacterized fungus was initially identified as a close relative to genera *Geomyces* and *Pseudogymnoascus* based on analyses of the internally transcribed spacer (ITS) region and small subunit ribosomal RNA gene sequences.[5,7] In 2009, it was classified and named *Geomyces destructans*, but was later reclassified as *Pseudogymnoascus destructans* in 2013 based on its distinctive morphology and repeated gene sequence analysis.[5,7,10] Initially, the presence of *Pd* was associated with WNS, but no strong evidence pointed towards the fungus as the causative agent of the disease. There was doubt, as the fungus was found in Europe with no associated disease and most fungal infections lead to immune system dysfunction—a feature not present in the pathogenesis of the WNS. However, in 2011, *Pd* was confirmed to be the causative agent of White-nose Syndrome by experimentally inoculating healthy *Myotis lucifugus* with pure cultures of *Pd*.

This inoculation successfully induced WNS in bats, and live *Pd* could be cultured from diseased bats, meeting the criteria of a primary pathogen.[11]

The fungal hyphae invade hair follicles, sebaceous glands, and apocrine glands. In the wings, the hyphae extend through the thin epidermis into the vascular and connective tissue. The colonization and invasion of the fungus prevents passive gas exchange across the wing membrane, causing an increase in blood CO_2, resulting in acidemia and hyperkalemia.[3,12] The interruption in passive respiration increases the rate of pulmonary respiration and low blood pH induces hyperventilation, which is both metabolically expensive and leads to increased pulmonary evaporative water loss. This leads to depletion of fat reserves, even before torpor patterns are disrupted.[12] Arousal is induced by dehydration and the acidemia, requiring the bat to reheat itself to euthermic temperatures, resume active pulmonary gas exchange, and forage for food and water. The arousal process further depletes fat stores prematurely, reducing the bats' chances of surviving through the winter period.[3,11–14]

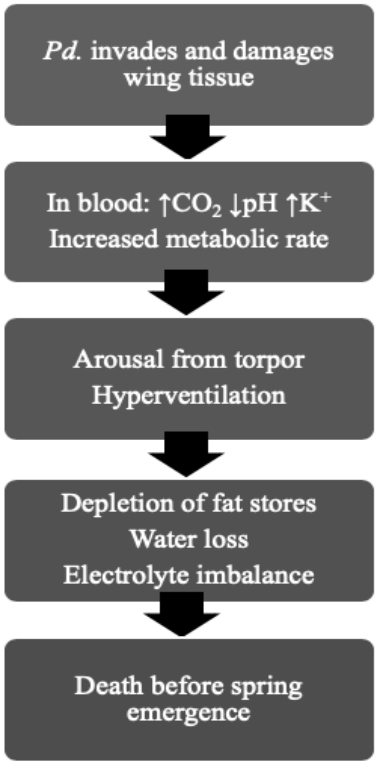

Figure 1. Disease cascade in bat White-nose Syndrome.[10]

The sudden population devastation and rapid spread of WNS through North America raised a critical question: what caused the 2006 WNS outbreak? Two hypotheses remained prevalent throughout the search for the origin of the disease: the endemic pathogen hypothesis and the novel pathogen hypothesis.[15] The endemic pathogen hypothesis states that *Pd* may have been a native fungus that, through genetic mutation,

developed characteristics causing it to be more pathogenic to bat populations. Whereas the novel pathogen hypothesis states that the fungus was an invasive species introduced to North America from a different geographical region.[16] The endemic pathogen hypothesis was challenged by the lack of species closely related to *Pd* for the fungus to have evolved from.[14] Furthermore, genotypic evidence suggest a clonal spread of *Pd* across the east coast to the Midwest, with only a single mating type, an unusual model for the natural development and spread of a native species.[17,18] In contrast, it has been determined that *Pd* is widespread in Europe with two mating types present to participate in sexual recombination by a heterothallic mating system—whereby different sexual structures exist in different individuals.[19–23] The most striking piece of evidence at the time, which altered the favoured hypothesis towards *Pd* being a novel pathogen in North America, was the lack of mass mortality in European hibernacula in the presence of the fungus. This evidence suggested a resistance to the fungus due to long exposure and coevolution of the *Pd* fungus and the bat species in the area.[19,24] To confirm that differences in pathogenicity between the European and North American strains was not causing the differences in mortality, North American bats were inoculated with European isolates of the fungus. This resulted in symptoms and mortality characteristic of White-nose Syndrome, revealing that the European fungus was also sufficient to induce the disease.[16] This not only provided evidence for the origin of the fungus, but also provided a model of study for *Pd* resistance in European bats, which could be applied to control spread and mortality in North American populations. Further evidence that pinpointed Europe as the specific site of origin was the presence of eight distinct haplotypes in Europe and only one present in North America (based on the presence of variation at eight loci); the most common haplotype in Europe

(Hap_1) is shared among all *Pd* isolates from Canada and the United States.[25] In-depth phylogenetic analysis and molecular dating of *Pd* strains from North America, Europe and Asia show distinct populations in Europe (with the North American isolates nested in this population), China, and Mongolia. Among the European population (including the North American isolates) diverged in the last century and diverged from the Asian populations over 3000 years ago.[26] This evidence confirms that, ancestrally, *Pd* originated in the Palaearctic region, and was only transferred to North America recently.

1.3 Resistance to White-nose Syndrome

To further understand the mechanism behind the European bat resistance, comprehensive investigation went into the immune function of unaffected and affected bats—both North American and European; these studies revealed surprising differences. It was determined that North American bat species mount an immune response despite immune downregulation in the torpid state.[27–32] Resistance to a pathogen requires a coordinated and adapted immune response, whereby innate immune mechanisms are regulated and targeted for an effective and appropriate response. While North American bats show evidence of immune system regulation, the decreased survival may be due to the lack of specificity, efficiency, and targeting in the mounted response.

In torpid bats, there is a characteristic lack of inflammation; however, upon arousal and return to a euthermic state, intense neutrophilic inflammation and emaciation of wing tissue is observed.[30,32] This has been attributed to an immune reconstitution inflammatory response, whereby an immunosuppressed host is infected, then upon the return to an immunocompetent state a severe immune response is mounted to combat the now-

established infection.[30] However, there is evidence of increased white blood cell and cytokine activity in affected bats, even while torpid.[27,31,32] Increased activation of cathelicidins, pro-inflammatory cytokines, and inflammatory response modulators reveal that an inflammatory response is being mounted but not effectively carried through.[31,32] One proposed issue is inappropriate targeting; the gene expression of these inflammation factors occur primarily in the lungs.[31] Thus far, there is no evidence that *Pd* infects the lungs; this response may be a non-specific host response to unknown fungal invasion or it may successfully be preventing establishment of spores in the lung tissue. Regardless, this response does not prevent infection and spread on the surface of the wings, as it is observed that, despite cytokine and chemokines being appropriately expressed, there is no recruitment of immune cells to the infection sites.[32]

Immune response comparison between affected and unaffected bats, as well as affected North American bats and European bats, reveal that antibody-mediated response cannot explain the resistance observed. Higher expression of anti-*Pd* antibodies was observed in affected North American bats than affected European bats, as well as decreased mass correlated with production of certain anti-*Pd* antibodies.[28,29] However, it should be noted, that infected bats that continue to successfully emerge from hibernation in regions of North America where *Pd* has been present longest also had higher antibody levels than emerging bats in more recently infected regions, providing little clarity to the role of antibodies in WNS resistance.[28] While evidence shows that classical host-immunity models may not be able to explain reduced severity of infection, there is evidence that micro-ecological defenses might.[29,33–39]

1.4 Microecological Defenses: Immune-Relevant Microbe-Microbe Interactions

While therapeutic agents for microbial pathogens have historically focused on diversified antimicrobials, probiotics may be the key in fighting infection by providing new models for treatment, as well as new sources of naturally-derived antimicrobials.[36] The scope of microorganisms that inhabit a host can be beneficial, benign, or pathogenic. These host-microbe relationships are not static; benign microbes of one host may become beneficial when introduced to another host, or they may become pathogenic. The host provides a habitat for the important microbe ecosystem that can provide protection from pathogen invasion. The term "immunobiome" describes the immune defenses provided by and shaped by microbes on the host organism, based on selective evolutionary and ecological pressure.[36]

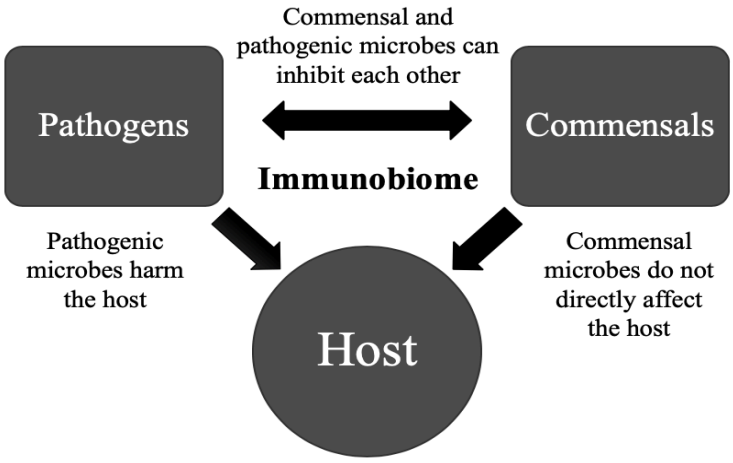

Figure 2. Microbe-host interactions in the immunobiome.

Microbial protection is due to metabolic secretions, which can nourish and contribute to host barriers, while others may act as antimicrobials to prevent competing microbes from colonizing and utilizing the same nutritional sources. This inhibition is a form of interference competition, whereby one organism uses a mechanism to prevent or slow other organisms from accessing shared resources. For this reason, microbes, especially those that inhabit hosts experiencing pathogen pressure (a strong competitor for resources), may be the key to new therapeutics for infection-based diseases, like WNS.

The first successful attempt at using microbe-derived treatments against *Pd* occurred in 2013, with bacterially produced volatile organic compounds (VOCs).[37] In 2013, Cornelison *et al.* used fungistatic VOCs previously described to be produced by soil bacteria, including decanal, nonanal, and benzaldehyde; all six tested VOCs showed successful inhibition of conidial growth and mycelial extension.[37] In 2014, Cornelison *et al.* continued studying volatile-based inhibition of *Pd*, this time investigating contact-independent inhibition with bacteria *Rhodococcus rhodochrous*, a soil-associated bacteria known to delay fruit ripening.[33] It was determined that induced *R. rhodochrous* caused complete inhibition of conidial growth in *Pd* when grown in a shared air-space. However, there are ecological concerns with the application of this treatment, as it would involve introduction of an endemic bacteria to an already fragile micro-ecosystem.

The use of cave-adjacent soil and substrate microbes has been investigated to resolve this problem; if the inhibitory microbe is native to the cave environment, using treatments derived from it may be better tolerated. In 2015, Zhang *et al.* isolated a novel *Trichoderma polysporum* strain from a cave affected by WNS.[35] Extracts from the strain not only showed marked inhibition of *Pd*, but also specific inhibition, as it did not inhibit the closely-related *Pseudogymnoascus pannorum*. The identity of the fungistatic compounds in the extract were not determined. In 2017, Micalizzi *et al.* of the M. Smith Lab at Carleton University (Ottawa, Canada) examined both contact-dependant and independent inhibition of *Pd* using strains sourced from various environmental substrates in cave areas.[39] Analysis of VOCs from inhibitory strains identified four bioactive volatiles: 2-methyl-1-propanol, 2-methyl-1-butanol, propanoic acid, and 1-pentanol. All four volatiles were tested directly against *Pd*, and complete inhibition occurred for all strains.

Contact-dependant strains were investigated in bioassays and spent-media tests, with several antagonist's spent media showing inhibition against *Pd*, but not closely related *P. pannorum* or *P. roseus.* These provide strong candidates for isolating effective and specific anti-*Pd* natural products. However, identification of the compounds from the spent media was hindered because the compounds were highly water soluble and difficult to separate out without affecting the activity.

In 2015, in an effort to find probiotic strains for direct treatment of WNS, Hoyt *et al.* isolated and investigated the anti-*Pd* activity of cutaneous bacteria directly off hibernating bats.[34] Six *Pseudomonas* isolates were tested for contact-dependent activity by coculturing against *Pd*, with two isolates showing optimal inhibition at all concentrations. In 2016, the efficacy of one of these *Pseudomonas* isolates called *Pf1* as an *in vivo* treatment was tested.[38] It was determined that, when the bat was inoculated concurrently with *Pf1* and *Pd* disease severity was reduced; disease severity was measured based on wing lesions, surface fungi, *Pd* load, UV fluorescence, and torpor bout duration. While simultaneous inoculation reduced severity, it was found that pre-treatment with *Pf1* actually increased severity.

Together, these investigations strongly suggest the efficacy of microbially-derived treatments for White-nose Syndrome. While direct probiotic treatment and VOCs may be viable solutions to treating the WNS problem, further investigation into isolating coculture-stimulated antimicrobial natural products may provide broader utility. Not only could they assist in treating other infectious diseases, but they could also lead to the development of more diversified antimicrobials—a necessity due to the rise of antimicrobial-resistant superbugs.

1.5 Objectives

The objectives of this study are to 1) create a microbial library derived from cutaneous samplings of WNS-resistant North American bat populations, 2) screen microbes for inhibitory activity against *Pd* and closely related species, and 3) identify the nature of any inhibition. By assessing bat populations that have shown some degree of resistance to the WNS epizootic, there is a greater expectation to find cutaneous microbial communities that are able to slow the growth of *Pd.* By co-culturing strains isolated from bats against the *Pd* fungus and other *Pseudogymnoascus (Pga)* species, it can be determined which strains are able to most effectively compete with the pathogen, visualized by inhibited growth. This inhibitory action will be assessed to determine whether it is specific to *Pd* or more generally anti-fungal, whether it is innate or induced, and whether it is based on resources competition or interference competition. Specificity will be assessed by comparing the degree of inhibitory activity in a pairwise assay against *Pd* with the inhibitory activity against three other *Pseudogymnoascus* species. To determine whether the inhibitory activity from pairwise testing is innate (produced by the pure strain without the threat of pathogen pressure) or induced (only produced when the strain senses nearby competitors), the metabolite profile of pure and pairwise grown strains will be compared to determine if novel molecules are produced as a result of co-culturing. Finally, to test whether competition is based on resources (growth inhibition based solely on the limited amount of space, nutrients, and carrying capacity of the environment) or interference (incendiary mechanisms to gain an advantage over competitors), *Pseudogymnoascus* fungi will be grown in the presence of metabolites extracted from pure isolated strains, without the cell component present to compete for resources.

2. Experimental

The following work was performed in a Containment Level 2 laboratory and executed according to Canadian Biosafety Standards and Guidelines. Active strain work was completed in a biological safety cabinet and all materials used were disposed of in sealed containers for subsequent incineration. The standard operating procedures for autoclave use, biological safety cabinet use, decontamination, and waste disposal are outlined in the Saint Mary's University Biosafety Manual.

2.1 Assembling and Characterizing a Strain Library

2.1.1 Sample Collection:

Agar slants made from 10% Reasoner's 2A (R2A) agar (HiMedia; 0.05g casein hydrolysate, 0.05g dextrose, 0.05g starch, 0.05g yeast extract, 0.03g dipotassium phosphate, 0.03g sodium pyruvate, 0.025g casein peptone, 0.025g meat peptone, 0.0024g magnesium sulfate, 15g agar powder, and 1000mL dH_2O) with pre-wetted (sterile dH_2O) sterile cotton swabs were sent to Dr. Paul Faure at the McMaster University Bat Lab. The Faure Group sampled *Eptesicus fuscus* (Big brown bats) by running one pre-wetted swab over the muzzle five times, and another swab over the forearms five times each (Fig 3). The swabs were used to inoculate the agar slants and sealed in the slant container for transport.

Figure 3. Sample collection from bat muzzle and forearm.

2.1.2 Strain Isolation:

Upon receiving inoculated agar slants, each swab was used to inoculate a 10% yeast malt agar (YMA: HiMedia; 0.3g yeast extract, 0.3g malt extract, 1g dextrose, 20g agar powder, and 1000mL dH_2O) plate and a 10% R2A plate (Fig 4A). The plates were incubated at 19°C for four weeks to maximize strain development and diversity (Fig 4B). All morphologically distinct colonies were isolated by restreaking and allowed to grow for three weeks at 19°C (Fig 4C). Strains that were morphologically similar were cocultured pairwise for comparison and allowed to grow for two weeks at 19°C. Strains were tested on selective media (containing 100µg/mL ampicillin or 10µg/mL cycloheximide) in order to further separate strains and understand the identity of each unknown strain. Based on gross and microscopic examination of morphology, similarity in growth patterns, and behaviour in cold and selective media conditions, strains that were considered redundant were grouped to reduce the number of working strains. All isolated strains were transferred to 10% YMA and grouped again. Each morphologically distinct strain was isolated at least twice more to achieve pure strains, with some strains requiring up to five restreaks to separate closely-growing strains. The 39 resulting strains obtained from the Faure Lab were labelled with an F-strain number (e.g. F1) and six strains determined to be lab-introduced contaminants were labelled with a C-strain number (e.g. C1). Eleven pure microbial strains were obtained from Dr. Myron Smith's lab at Carleton

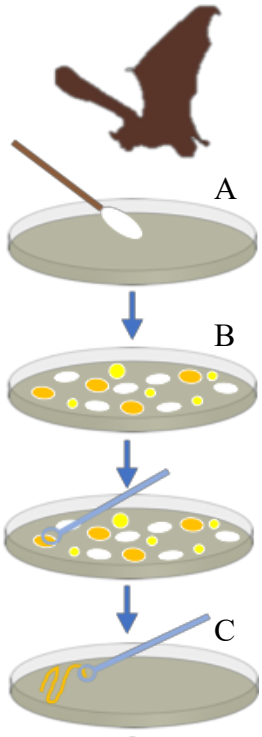

Figure 4. Strain isolation process.

University; these strains were labelled with an S-strain number (e.g. S1). The growth progression was tracked and described for two weeks.

Concentrated strain-inoculated liquid media stocks were made by placing 1mL of 100% yeast malt broth (YMB: HiMedia; 3g yeast extract, 3g malt extract, 10g dextrose, and 1000mL dH_2O) on an agar plate containing a pure strain after at least one week of growth (Fig 5A). The surface of the plate was scraped with an inoculating loop to disturb and detach bacteria/fungi and disperse it in the broth (Fig 5B). The broth containing the microbes was transferred to a sterile cryovial (Fig 5C). Due to large fungal clusters preventing an even distribution in the broth, optical density could not be accurately determined. These concentrated stocks were used for direct plating onto agar, for making working stocks in a 1:10 dilution in 100% YMB, and for making frozen stocks in a 1:1 dilution in 50% glycerol (kept at -80°C for long term storage).

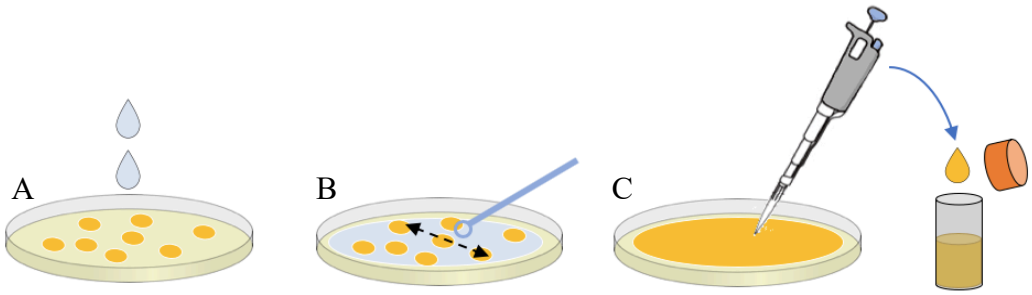

Figure 5. Preparation of a concentrated stock

2.1.3 Optimal Temperature Testing:

All strains were inoculated (10µL of conc. strain-inoculated liquid media) on a single well in three sets of 24 well plates (well diameter: 1.5cm) containing 100% YMA (HiMedia; 3g yeast extract, 3g malt extract, 10g dextrose, 20g agar powder, and 1000mL). Each plate set was incubated at 12°C, RT (19-21°C), and 30°C. Growth was measured on

Day 1 and Day 7. Temperature growth was scored from 0 to 3; a score of 3 signified strong growth (colony diameter > 1cm), a score of 2 signified moderate growth (0.5cm < colony diameter < 1cm), a score of 1 signified poor growth (colony diameter < 0.5cm but growth is still visible), and a score of 0 signified no growth (where no growth could be observed). Strains showing moderate to strong growth at 12°C were considered psychrotolerant.

2.2 Preliminary Pairwise Testing

The compiled strain library was tested pairwise against four species of *Pseudogymnoascus* fungi (Fig 6): *Pseudogymnoascus bhatti (Pb), Pseudogymnoascus destructans (Pd), Geomyces (Pseudogymnoascus) pannorum (Pp), and Pseudogymnoascus roseus (Pr)*. Based on measured growth of the *Pseudogymnoascus* strains at 12°C and 19°C, *Pd* and *Pr* were used for pairwise testing at 12°C against psychrotolerant strains, while *Pb* and *Pp* were used for pairwise testing against the whole strain library (consisting of the F-strains, S-strains, and C-strains) at 19°C. Pairwise testing at 30°C did not take place due to the lack of growth of any of the *P*-strains at this temperature.

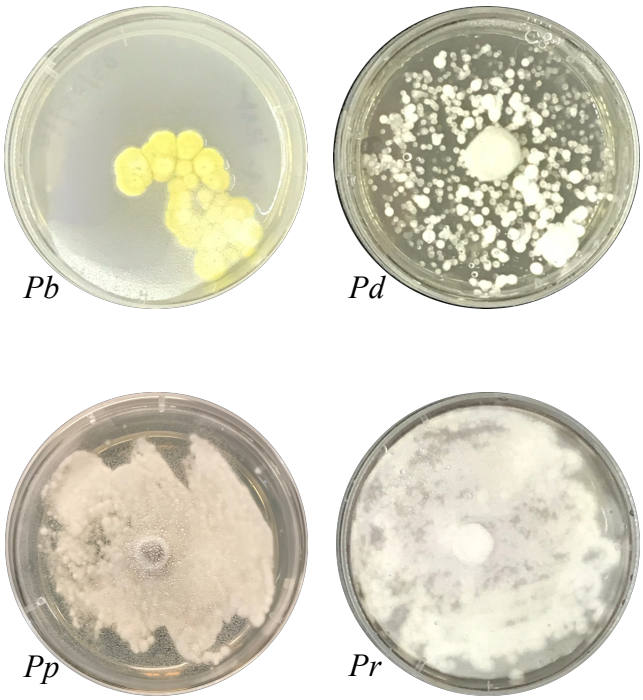

Figure 6. Morphology of *Pseudogymnoascus* species

Pseudogymnoascus strains (*P*-strains) were inoculated on the plate (25µL of conc. liquid stock) and allowed to establish colonies (3 days for *Pb/Pp*, 5 days for *Pd/Pr*). This is due to the slow growing nature of each of the *P*-strains. Sample strains were inoculated (25µL of conc. liquid stock) opposite to the pre-established colonies of a *P*-strain (Fig 7). Colony size, zone of inhibition, and *P*-strain growth were measured to determine the presence of inhibitory activity after 7 days. The growth of the pairwise *P*-strains and pure *P*-strains were used to quantify and compare inhibitory effects. The mean colony size of the *P*-strain in the pairwise test (performed in triplicate) was determined and compared to the mean colony size of the pure *P*-strain (from 48 replicates) in the same growth conditions and timeframe by determining the difference between the values and dividing by pure growth to determine a percent inhibition. Percent inhibition was scored from 0 to 3; a score of 3 signified strong inhibition (75% < %inhibition ≤ 100%), a score of 2 signified moderate inhibition (50% < %inhibition ≤ 75%), a score of 1 signified limited inhibition (25% < %inhibition ≤ 50%), and a score of 0 signified no inhibition (inhibition ≤ 25%). This process was used to determine which strains showed the most promising overall activity against the *P*-strains; only these strains were used for further analysis.

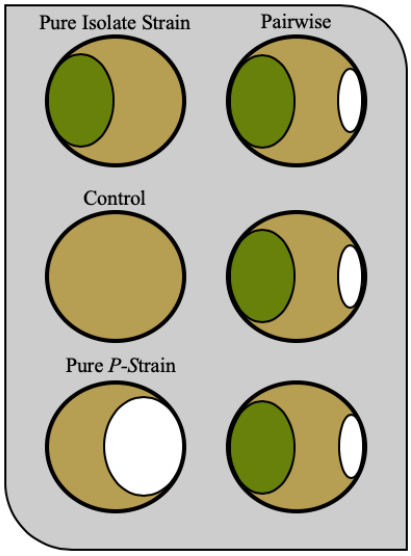

Figure 7. Layout of a pairwise test plate.

2.3 Extraction and Fractionation of Metabolites

To isolate metabolites from the media of pure and pairwise assays, strains were grown on a large scale on 100% YMA on 12-well plates (the number of plates used is dependent on purpose of extraction). The discs of spent media (4mL, 2cm in diameter) were removed from the plates and extracted three times with an equal volume of an 85:15 ethyl acetate-methanol solution for 2 hours each (Fig 8). The solvent was gravity filtered to remove most particulate matter and transferred to a round bottom flask. The solvent was evaporated off (by rotary evaporation) and the solid was re-dissolved in ~5ml of MeOH and transferred to a pre-weighed vial through a 0.22micron filter to remove cells. The solvent was evaporated off and made up to 10mg/mL in HPLC-grade methanol. This was completed for the selected pure isolate strains (F1, F3, S2, S8, and S9), the *P*-strains, and the pairwise tests between each of the isolate strains and *P*-strains.

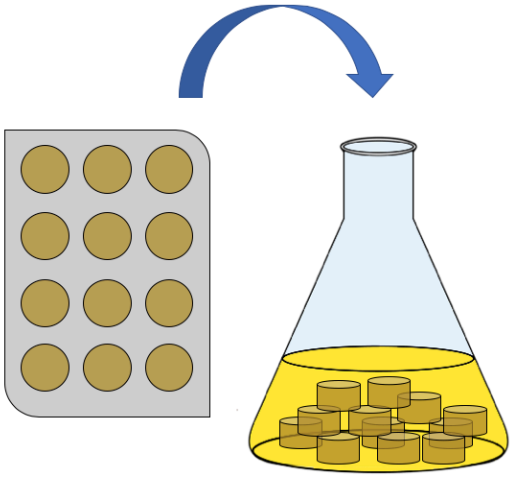

Figure 8. Extraction of media from a 12 well plate.

The crude extract of each of the pure isolate strain (1mL of 10mg/mL in methanol) was fractionated using a gravity microcolumn with C18 silica (4cm height, approximately 0.75g) and an acetonitrile/water gradient (10mL each of 0%, 10%, 20%, 50%, 80%, and 100% acetonitrile in water). Each fraction was collected in scintillation vials and stored at room temperature for subsequent bioactivity testing and analysis.

2.4 Analysis of Extracts and Fractions

To prepare for liquid chromatography (paired with mass spectrometry and a diode array detector; LC/MS/DAD), crude extracts were diluted to 5mg/mL in HPLC-grade methanol. Pure methanol and an extract of an uninoculated agar plate were used as controls. Crude extracts were analyzed using an Agilent 1100 series LC-MS equipped with an ion-trap mass spectrometer (Agilent 110 Series LC/MSD Trap) and a diode array detector. The method utilized reverse phase liquid chromatography with a C18 column (Zorbax Eclipse XDB 80Å C18, 4.6 x 75mm, 3.5µm HPLC column). Fractions were eluted starting with 20% acetonitrile (ACN) with 0.1% formic acid in deionized water (dH_2O) with 0.1% formic acid for 25 min followed by 80% ACN (with 0.1% formic acid) in dH_2O for 3min, then 100% ACN (with 0.1% formic acid) for 5 min. A diode array detector was used to collect a full range chromatogram (190-400nm) and a chromatogram at wavelengths 212nm, 225nm, 254nm, 275nm, and 350nm to detect the presence of compounds. Positive-mode electrospray ionization mass spectrometry was used to further detect and resolve compounds in the crude extract from 100m/z to 2200m/z. This was performed to obtain a broad overview of the compounds produced by the inhibitory strains, both while pure and paired with each *Pseudogymnoascus* strain, to determine if any novel metabolites are being induced by pairwise growth. The choice of column composition and mobile phase components were based on the *Trichoderma polysporum* metabolite separation performed by Zhang et al.[35]; the method was optimized for general separation of fungal metabolites with the help of Patricia Granados at the Saint Mary's University Centre for Environmental Analysis and Remediation (CEAR) Lab, Halifax, NS.

2.5 Assessing Bioactivity of Extracted Metabolites

2.5.1 Isolate-Supplemented Media Testing:

In order to assess whether inhibition occurred by interference competition (use of inhibitory metabolites), as opposed to resource competition (inhibition by deprivation of resources), the growth of each *P*-strain was observed on media supplemented with the cell-free extracts of the isolate strains. Upscaled growth of pure isolate strains occurred by inoculating five 12-well plates per strain—approximately 250mL of 100% YMA media. These plates underwent extraction and were made up to a stock concentration (10mg/mL) in methanol (Fig 9A). A subsequent batch of 100% YMA media was supplemented with the extract solution with a starting concentration of 100µg/mL extract in media (Fig 9B). *P*-strains were inoculated on the plates (Fig 9C) and degree of inhibition was based on coverage of the plate with *P*-strain fungus. A control plate was made for each *P*-strain by supplementing the media with 10mL of methanol per 1L of agar to ensure methanol was not limiting the growth of the strains.

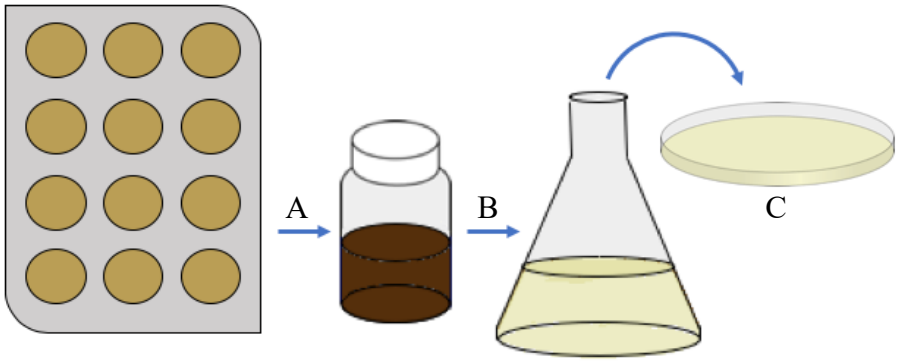

Figure 9. Supplementation of media with an isolate strain extract.

After 10 days of growth, plate coverage was quantified with the ImageJ plugin ColonyArea, which measures the percent coverage based on coloration and color intensity of a photographed plate.[40,41] The pathway used in the program is as followed: Plugins > ColonyArea > colony area > Input=1, row=1, column=1 > Plugins > ColonyArea > colony threshold > Plugin > ColonyArea> colony measure. Since the *P*-strain growth was considered the negative space due to its white colouration the Area Percent was subtracted from 100 to determine colony coverage. Percent coverage was scored from 0 to 3; a score of 3 signified full coverage (75% < % coverage ≤ 100%), a score of 2 signified moderate coverage (50% < % coverage ≤ 75%), a score of 1 signified reduced coverage (25% < % coverage ≤ 50%), and a score of 0 signified limited coverage (% coverage ≤ 25%). Reduced and limited coverage of the *P*-strain on isolate supplement media indicated partial to complete inhibition.

Isolate strain S9 showed significant inhibitory activity in the initial supplemented media test (Fig 10A), so the media from each *P*-strain and control was extracted from the plate used for supplemented testing (Fig 10B). The extract was made up to 10mg/mL and used to re-supplement another round of media (Fig 10C), on which the appropriate *P*-strain was grown again (Fig 10D). The extraction and supplementation processes were completed once more for a total of three rounds (LC data was not collected after the third round). This process was used to assess the stability and continued bioactivity of the compounds produced by S9.

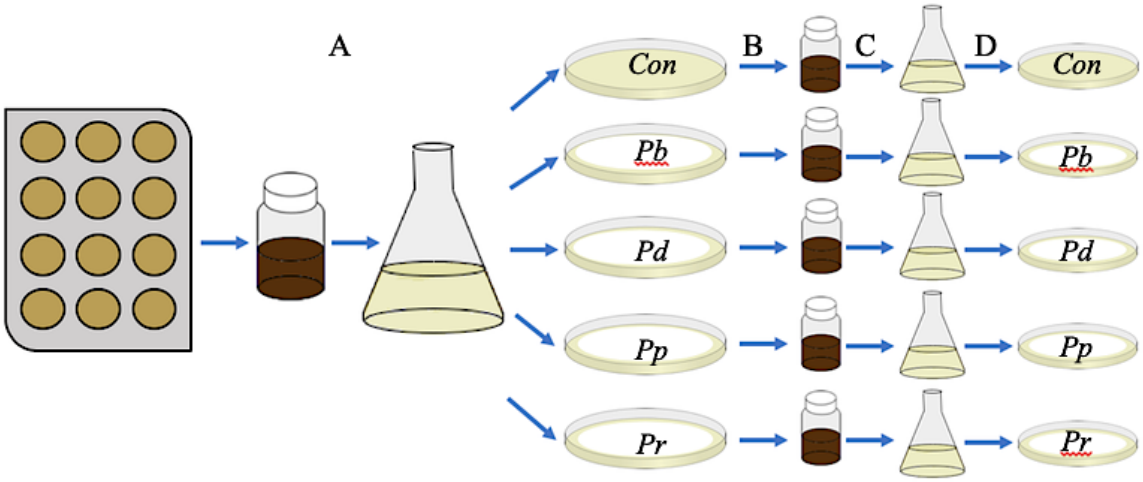

Figure 10. Consecutive extraction and supplementation of S9 metabolites in *P*-strain media

2.5.2 Disc Diffusion Assay:

Crude extracts and fractions were tested directly against the *P*-strains to determine which fraction(s) contain the bioactive molecule of interest for future compound isolation. Autoclaved circular discs (6mm diameter, Whatman Grade 1 Qualitative Filter Paper) were placed on 100% YMA media freshly inoculated with each *P*-strain (Fig 11A), then 10µL of crude extract or fraction was placed on the disc to allow it to absorb and diffuse outward into the media (Fig 11B; where *=crude, 1= 0% ACN, 2= 10% ACN, 3= 20% ACN, 4= 50% ACN, 5= 80% ACN, and 6=100% ACN fractions). Plates were made up in triplicate and a control plate was made for each strain using 10µL of methanol for the crude and each respective acetonitrile in water solution to determine if the solvent had any effect on the *P*-strain fungi. After 10 days of growth, the radii of the zone of inhibition around the discs were measured and averaged among the three trials (Fig 11C). The zone of inhibition was scored from 0 to 3; a score of 3 signified a distinct zone of inhibition (5mm < ZOI), a score

of 2 signified a moderate zone of inhibition (2.5mm < ZOI ≤ 5mm), a score of 1 signified a visible zone of inhibition (0.5mm < ZOI ≤ 2.5mm), and a score of 0 signified no zone of inhibition (ZOI ≤ 0.5mm).

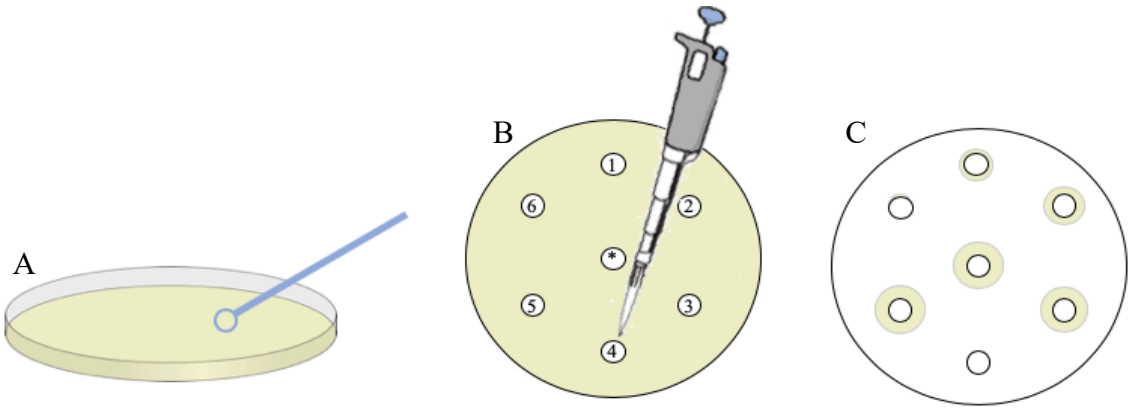

Figure 11. Preparation and layout of a disc diffusion assay experiment.

3. Results and Discussion

3.1 Assembling and Characterizing a Strain Library

3.1.1 Sample Collection:

The Faure Group at the McMaster Bat Lab sampled 40 healthy *Eptesicus fuscus.* Of the bats sampled, there were 29 adults (21 females, 8 males), which were captured near Molesworth, Ontario and 11 juveniles (4 females, 7 males), which were bred in captivity (Appendix A, Table A1). The muzzle samples from one of the adult females (P89) was not taken or was lost in transit, and the forearm swab showed no growth, thus it was excluded from remaining trials. Eleven pure strains were obtained from Dr. Myron Smith's lab. Each of these strains was shown to have activity against at least one of the *P*-strains by the Smith lab[39]; however, they had limited success at extracting stable bioactive compounds from the media for analysis.

3.1.2 Strain Isolation:

From the initial plates streaked, 179 strains were isolated (91 from YMA, 88 from R2A). Based on appearance and growth throughout three weeks, strains that appeared redundant were cocultured, and the strains confirmed to be redundant were grouped under a common strain number. This resulted in 127 strains (55 from YMA, 72 from R2A). Each strain was grown on selective media and this information, along with gross observation, was used to further group redundant strains. This resulted in 71 strains (39 From YMA, 32 from R2A). After all strains were transferred to YMA, strain growth at various temperatures and on selective media was tested again; this resulted in 39 non-redundant strains called the F-strains. With the addition of the 11 Smith Lab strains, or the S-strains, and 6 Contaminant Strains (strains found in later isolates and determined to be contaminants resulting from human error), C-strains, the isolate final library used for testing consisted of 56 unique strains and 4 *P*-strains (Appendix A, Table A2).

3.1.3 Optimal Temperature Testing:

Of the 56 strains, 39 strains grew at 12°C, 56 strains grew at room temperature (approximately 19-21°C), and 54 strains grew at 30°C (Table 1; Growth Score >1 considered sufficient growth). Of the *P*-Strains, *Pd* and *Pr* grow optimally at 12°C, *Pb* grow optimally at RT, and *Pp* grew equally well at 12 and RT.

Table 1. Heatmap of temperature-based growth data for entire strain library

Strain	Temp. Growth Score* 12°C	19°C	30°C	Strain	Temp. Growth Score* 12°C	19°C	30°C	Strain	Temp. Growth Score* 12°C	19°C	30°C
F1				F21				S2			
F2				F22				S3			
F3				F23				S4			
F4				F24				S5			
F5				F25				S6			
F6				F26				S7			
F7				F27				S8			
F8				F28				S9			
F9				F29				S10			
F10				F30				S11			
F11				F31				C1			
F12				F32				C2			
F13				F33				C3			
F14				F34				C4			
F15				F35				C5			
F16				F36				C6			
F17				F37				*Pb*			
F18				F38				*Pd*			
F19				F39				*Pp*			
F20				S1				*Pr*			

*Temperature Growth Scale: 0 | 1 | 2 | 3

3.2 Preliminary Pairwise Testing

All 50 F- and S-strains were pairwise tested at room temperature against *Pb* and *Pp*. Seven strains showed strong inhibition (>75%) against *Pb* and 11 strains showed strong inhibition against *Pp*. The 33 psychrotolerant strains were tested against *Pd* and *Pr* at 12°C. Nine strains showed strong inhibition (>75%) against *Pd* and 8 strains showed strong inhibition against *Pr* (Fig 12; Table 2). The strains that performed best at room temperature were F1, F3, F14, F24, F31, F39, S2, S8, S9, and S11; the strains that performed best at 12°C were F1, F3, F5, F38, S1, S2, S5, S8, S9, and S11. The strains F1, F3, S2, S8, and S9 (Fig 13) showed at least partial inhibition against each *P*-strain, with the highest overall combined scores; these strains were used for all subsequent analyses. The nature of the inhibition of these strains based on preliminary pairwise testing could have been either resource or interference based, and either innate or induced. Regardless, these five strains presented the best potential in the current strain library for finding novel antifungals, or even known antifungals with previously uncharacterized action against *Pd*.

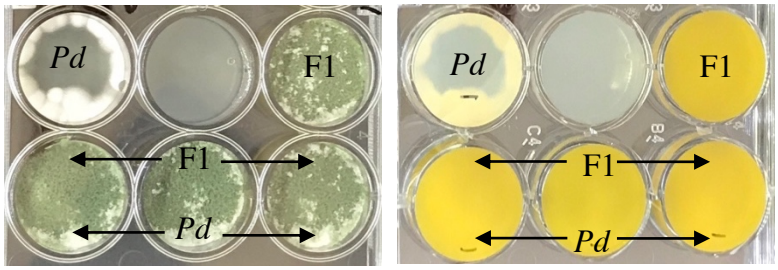

Figure 12. Observed pairwise inhibition between F1 and *Pd* (Right: top view; Left: reverse image of bottom view)

Figure 13. Morphology of selected isolate strains

Table 2. Inhibition heatmap of preliminary pairwise testing of the strain library against *P*-strains with *Pb* and *Pp* trials at room temperature and *Pd* and *Pr* trials at 12°C

Strain	Pairwise Inhibition Score*				Strain	Pairwise Inhibition Score*			
	Pb	***Pd***	***Pp***	***Pr***		***Pb***	***Pd***	***Pp***	***Pr***
F1	3	1	3	3	F26	0	0	1	0
F2	1	1	3	1	F27	0	2	0	1
F3	3	1	2	2	F28	0	1	0	2
F4	0	1	0	1	F29	0	NoData	0	NoData
F5	3	3	0	3	F30	0	NoData	1	NoData
F6	0	2	0	2	F31	2	2	3	3
F7	1	NoData	3	NoData	F32	0	NoData	0	NoData
F8	2	NoData	2	NoData	F33	0	NoData	1	NoData
F9	1	NoData	2	NoData	F34	1	2	3	2
F10	0	NoData	0	NoData	F35	1	3	0	2
F11	1	2	1	2	F36	1	NoData	3	NoData
F12	0	NoData	2	NoData	F37	1	NoData	1	NoData
F13	0	0	1	2	F38	1	2	3	3
F14	3	NoData	2	NoData	F39	2	2	3	3
F15	0	1	2	2	S1	2	3	2	2
F16	0	NoData	1	NoData	S2	3	3	2	3
F17	1	NoData	0	NoData	S3	0	NoData	1	NoData
F18	0	3	2	2	S4	0	2	0	1
F19	0	2	1	1	S5	3	3	0	2
F20	1	3	2	1	S6	0	NoData	0	NoData
F21	0	NoData	2	NoData	S7	0	2	2	1
F22	1	1	1	1	S8	2	2	3	2
F23	0	0	0	0	S9	3	3	2	2
F24	2	2	3	3	S10	0	0	1	1
F25	0	0	0	0	S11	1	3	3	3

*Inhibition Scale: No Data | 0 | 1 | 2 | 3

3.3 Analysis of Crude Extracts

After two weeks of growth on 250mL of 100% YMA media, the metabolites of the pure isolate strains (F1, F3, S2, S8, and S9; Fig 14), pure *P*-strains, pairwise inoculations of the isolate and *P*-strains, and an agar control were extracted and made up to 10mg/mL in methanol. The pairwise samples S2xPb, S2xPp, S9xPb, and S9xPp had to be regrown, and could only be grown for one week before extraction, resulting in a weaker yield, and a concentration of only 1mg/mL for LC analysis. LC/MS/DAD was run on the pure strains *P*-strains, an agar control sample, and a methanol control (Appendix B, Fig B1-B2), as well as each pure and pairwise isolate strains (Appendix B, Fig B3-B7); the total ion chromatogram and full-range (190-400nm) UV chromatogram were obtained for comparison. By comparing the pure isolate and *P*-strain chromatograms, unique signals in the pairwise sample were noted (Fig 15). Table 3 summarizes the number of unique signals in the media extracted from the pairwise plates.

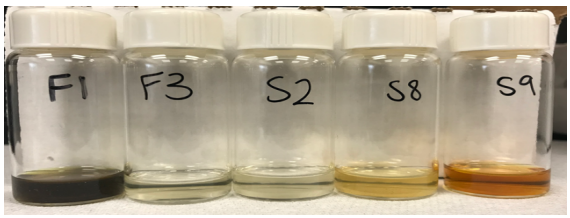

Figure 14. Crude extracts of selected strains.

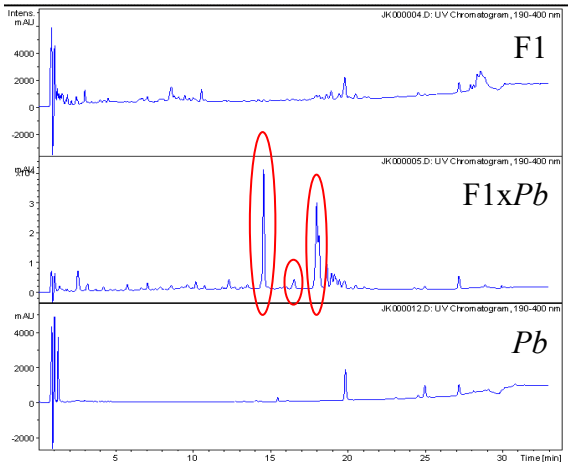

Figure 15. Stacked UV chromatogram for signal comparison

Table 3. Number of unique signals induced by the pairwise culturing of isolate and *P*-strains with *Pb* and *Pp* trials grown at room temperature and *Pd* and *Pr* trials grown at 12°C

Pairwise Strains	# Unique Signals Induced			
	Pb	***Pd***	***Pp***	***Pr***
F1	3	3	6	2
F3	0	1	0	2
S2	2	2	0	0
S8	0	0	0	2
S9	0	0	0	0

Due to the decreased growth time and metabolite concentration, the spectra of pairwise samples S2xPb, S2xPp, S9xPb, and S9xPp yielded low intensity signals, making accurate compound comparison difficult. Based on the number and intensity of unique signals in the F1 pairwise spectra, compounds were likely induced by the stress of co-culturing (Appendix B, Fig B3). However, whether or not the induced compounds have antifungal activity, and whether the unique compounds were produced by the isolate or the *P*-strain cannot be determined based on this method. Isolate strains F3, S2, S8, and S9 show few or very low intensity signals unique to the pure isolate and *P*-strain spectra, meaning novel metabolites were likely not induced under the co-culturing circumstances (Appendix B, Fig B4-B7). The retention times and relative intensities of induced peaks were reported in Appendix A, Table A3.

3.4 Assessing Bioactivity of Extracted Metabolites

3.4.1 Isolate-Supplemented Media Testing:

Each isolate-supplement media testing slowed the health and rate of growth of every *P*-strain in the first seven days compared to the control. However, after ten days of growth, the F3 and S8 supplemented media did not show any significant difference in coverage from the control for any of the *P*-strains. F1 and S2 supplemented media both inhibited *Pd* moderately, but neither had a significant effect on the other three *P*-strains. S9 supplemented media showed moderate inhibition of both *Pp* and *Pr*, and complete inhibition of both *Pb* and *Pd* (Table 4).

Table 4. Heatmap of *P*-strain plate coverage on isolate-supplemented media

Isolate Supplement	**Coverage Score***			
	Pb	***Pd***	***Pp***	***Pr***
F1				
F3				
S2				
S8				
S9				
C				
*Coverage Scale:	0	1	2	3

The lack of strong overall inhibition by strains F1, F3, S2, and S8 suggest that none of them have significant innate antifungal metabolite production that is active against *Pseudogymnoascus* fungi. This indicates that the inhibition observed in the preliminary trials may have been a result of resource-limited condition where the isolate strains out-competed the *P*-strains, as opposed to true metabolite-based interference competition. However, this along with the LC/MS/DAD data suggests that in the case of F1, it is possible

that this type of interference is being induced in co-culture conditions. Nevertheless, S9 appears to have significant innate activity, specifically towards *Pb* and *Pd*.

It was determined that the compounds produced by S9 were able to prevent the growth of *Pb* and *Pd* for at least 8 weeks (at which point the media began to dehydrate and crack) when supplemented into the media. In the consecutive extractions and supplementations using S9 metabolites, all four *P*-strains were inhibited in the first round (R1). After extraction and re-supplementation (R2), S9 metabolites retained activity against *Pb* and *Pd*, but lost some activity against *Pp* and *Pr*. After the final extraction and supplementation (R3), activity was retained against *Pb* and *Pd* but completely lost in *Pp* and *Pr* (Table 5). LS/MS/DAD analysis of the initial extract and extracts from R1 and R2 plates showed that the metabolite profile did not change from the initial extract to the R1 extraction. However, the metabolite profile diminished after the R2 extraction in *Pp* and *Pr*, but not *Pb* and *Pd* (Appendix B, Fig B8-B12).

Table 5. *P*-strain plate coverage on consecutive S9-supplemented media tests

S9 Supplement	**Coverage Score***			
	Pb	***Pd***	***Pp***	***Pr***
R1 S9				
R1 Control				
R2 S9				
R2 Control				
R3 S9				
R3 Control				
*Coverage Scale:	0	1	2	3

The specific and ongoing inhibition of *Pb* and *Pd,* and limited inhibition of *Pp* and *Pr* was observed again. However, the chromatograms give evidence as to reason for the decreased activity against *Pp* and *Pr*; the metabolite profile after the extraction from the

second round of supplemented media tests revealed that the *Pp* and *Pr* media were missing a distinct peak that eluted at 17.7min. This peak was present in the controls for each round and in the *Pb* and *Pd* media, but appears to have been degraded by *Pp* and *Pr*. It should be noted, that S9, *Pp,* and *Pr* were all isolated from hibernacula-adjacent environments and have likely coevolved, allowing these *P*-strains to develop mechanisms to combat or reduce the effect of the S9 antifungal compounds. However, S9 evolved independently from *Pb* and *Pd*, therefore its antifungal defences may be more effective against these strains. Overall, this result suggests that the compound eluting out at 17.7min is not only very stable (able to be extracted out of media at least three times) but may be the compound responsible for the innate antifungal action of S9 and will be a focus moving forward. The retention times, relative intensities of induced peaks, and associated masses were reported in Appendix A, Table A4. Higher resolution mass spectrometry is required to gain meaningful information about the composition and structure of the unknown compounds.

3.4.2 Disc Diffusion Assay:

After ten days of growth, the *P*-strain fungi overtook the plates with only a few discs showing visible zones of inhibition (Table 6). Most observed zones of inhibition were minimal, with just 1mm of visible inhibition from the edge of the discs. The only moderate to distinct zones of inhibition were due to the crude S9 extracts against *Pb* and *Pd* and the sixth fraction (100% ACN) of S9 on *Pd*. The inhibition of *Pb* and *Pd* by the crude S9 sample was expected due to the innate activity observed in the supplemented media tests. However, the moderate zone of inhibition around the 100% ACN disc supports the prediction that the bioactive metabolite is likely one that eluted out in the later stages of the

LC run (possibly 17.7min). The minimal results for the crude and fractionated samples of F1, F3, S2 and S8 could be due to the lack of innate antifungal activity (also observed in the supplemented media tests) and the extremely low concentration of metabolites each solvent after fractionation.

Table 6. Zone of inhibition of *P*-strains on disc diffusion assays

Fraction	Zone of Inhibition Score*				Fraction	Zone of Inhibition Score*			
	Pb	***Pd***	***Pp***	***Pr***		***Pb***	***Pd***	***Pp***	***Pr***
Crude F1					Crude S8				
F1 Fraction 1					S8 Fraction 1				
F1 Fraction 2					S8 Fraction 2				
F1 Fraction 3					S8 Fraction 3				
F1 Fraction 4					S8 Fraction 4				
F1 Fraction 5					S8 Fraction 5				
F1 Fraction 6					S8 Fraction 6				
Crude F3					Crude S9				
F3 Fraction 1					S9 Fraction 1				
F3 Fraction 2					S9 Fraction 2				
F3 Fraction 3					S9 Fraction 3				
F3 Fraction 4					S9 Fraction 4				
F3 Fraction 5					S9 Fraction 5				
F3 Fraction 6					S9 Fraction 6				
Crude S2					Control MeOH				
S2 Fraction 1					Control Fraction 1				
S2 Fraction 2					Control Fraction 2				
S2 Fraction 3					Control Fraction 3				
S2 Fraction 4					Control Fraction 4				
S2 Fraction 5					Control Fraction 5				
S2 Fraction 6					Control Fraction 6				

*Zone of Inhibition Scale: 0 | 1 | 2 | 3

4. Conclusion

In summary, it was shown that microbes isolated from bats and their hibernacula environments can have potent antimicrobial activity against *Pseudogymnoascus destructans* and closely related species. While in-depth analysis was only performed on five strains, a library consisting of 56 microbes associated with the North American bat species, *Eptesicus fuscus,* has been created, with multiple candidates also showing some degree of antifungal activity. Of the five strains analyzed, three (F3, S2, and S8) appear to be able to effectively compete with *Pd* and other *Pga* species for limited resources, if not by any interference mechanism. One strain (F1) shows evidence of producing potentially antifungal metabolites by induction when under the stress of coculture conditions. The final strain (S9) shows potent and innate antifungal activity, with specificity toward unfamiliar fungi (such as the invasive *Pd*).

The key strength of this investigation was the development of standardized processes to screen for and determine mode of inhibition. The extraction process applied was able to remove metabolites from spent media for analysis without degradation and while maintaining bioactivity. However, the investigation fell short of isolating and identifying pure bioactive compounds. The main reason for this was the limitation of time, the extremely low metabolite yields, and the rudimentary nature of the fractionation process used. At no point were pure compounds able to be separated, preventing analysis with IR and NMR, and the resolution of the mass spectrometer prevented any compositional or structural information from being determined.

5. Future Work

To further this investigation, the methods of purification and elucidation must be developed. Rather than manually fractionating, one dimension of a 2D LC could be used to separate and collect fractions based on detected signals, as opposed to approximate gradient composition. This would separate the crude extract in a more refined way, leading to a simpler purification process for samples; this would allow for IR and NMR analysis on the samples for identification or, in the case of a novel compound, elucidation. Adapting the current LC/MS method for use on a high-resolution mass spectrometer would help to determine the exact mass of compounds, making it easier to determine chemical composition and structure based on fragmentation and allow for more targeted searches in natural products databases. Once purified, the degree of bioactivity, the presence of synergistic effects, and the mechanism of action can also be deduced.

To increase the potential discovery of antifungal compounds, the remaining candidates from the microbial library should be screened to determine if any other strains show bioactivity past the preliminary co-culture. Furthermore, methods of inducing metabolites could be expanded beyond simple co-culturing; by altering nutritional availability, introducing an artificial scaffolding to mimic the surface of bat skin, and introducing stressors such as changes in salt content, pH, and moisture levels, a larger variety of compounds with potential activity may be induced. Acquiring and screening microbes derived from European bats and hibernacula may yield more anti-*Pd* compounds due to the coevolution of European bats and the *Pd* fungus.

Finally, the identity of the microbes in the strain library should be determined. Then, the genome can be used to determine the biosynthetic pathways of elucidated antifungals and mined to search for silent genes, which may be activated by induction.

6. Reference:

(1) Carey, H. V.; Andrews, M. T.; Martin, S. L. Mammalian Hibernation: Cellular and Molecular Responses to Depressed Metabolism and Low Temperature. *Physiological Reviews* **2003**, *83* (4), 1153–1181. https://doi.org/10.1152/physrev.00008.2003.

(2) Cryan, P. M.; Meteyer, C.; Boyles, J. G.; Blehert, D. S. Wing Pathology of White-Nose Syndrome in Bats Suggests Life-Threatening Disruption of Physiology. *BMC Biology* **2010**, *8* (1), 135. https://doi.org/10.1186/1741-7007-8-135.

(3) Makanya, A. N.; Mortola, J. P. The Structural Design of the Bat Wing Web and Its Possible Role in Gas Exchange. *Journal of Anatomy* **2007**, *211* (6), 687–697. https://doi.org/10.1111/j.1469-7580.2007.00817.x.

(4) U.S. Fish & Wildlife Service. *White-Nose Syndrome: The Devastating Disease of Hibernating Bats in North America April 2017*; 2017.

(5) Blehert, D. S.; Hicks, A. C.; Behr, M.; Meteyer, C. U.; Berlowski-Zier, B. M.; Buckles, E. L.; Coleman, J. T. H.; Darling, S. R.; Gargas, A.; Niver, R.; et al. Bat White-Nose Syndrome: An Emerging Fungal Pathogen? *Science* **2009**, *323* (5911), 227. https://doi.org/10.1126/science.1163874.

(6) U.S. Fish & Wildlife Service. *White-Nose Syndrome Occurrence Map: Updated Oct 1, 2018*; 2018.

(7) Gargas, A.; Trest, M.; Christensen, M.; Volk, T. J.; Blehert, D. S. *Geomyces destructans Sp. Nov. Associated with Bat White-Nose Syndrome. Mycotaxon*; 2009; Vol. 108.

(8) Frick, W. F.; Pollock, J. F.; Hicks, A. C.; Langwig, K. E.; Reynolds, D. S.; Turner, G. G.; Butchkoski, C. M.; Kunz, T. H. An Emerging Disease Causes Regional Population Collapse of a Common North American Bat Species. *Science* **2010**, *329* (5992), 679. https://doi.org/10.1126/science.1188594.

(9) Meteyer, C. U.; Buckles, E. L.; Blehert, D. S.; Hicks, A. C.; Green, D. E.; Shearn-Bochsler, V.; Thomas, N. J.; Gargas, A.; Behr, M. J. Histopathologic Criteria to Confirm White-Nose Syndrome in Bats. *J VET Diagn Invest* **2009**, *21* (4), 411–414. https://doi.org/10.1177/104063870902100401.

(10) Verant, M. L.; Meteyer, C. U.; Speakman, J. R.; Cryan, P. M.; Lorch, J. M.; Blehert, D. S. White-Nose Syndrome Initiates a Cascade of Physiologic Disturbances in the Hibernating Bat Host. *BMC Physiology* **2014**, *14* (1). https://doi.org/10.1186/s12899-014-0010-4.

(11) Reeder, D. M.; Frank, C. L.; Turner, G. G.; Meteyer, C. U.; Kurta, A.; Britzke, E. R.; Vodzak, M. E.; Darling, S. R.; Stihler, C. W.; Hicks, A. C.; et al. Frequent Arousal from Hibernation Linked to Severity of Infection and Mortality in Bats with White-Nose Syndrome. *PLoS ONE* **2012**, *7* (6), e38920. https://doi.org/10.1371/journal.pone.0038920.

(12) Warnecke, L.; Turner, J. M.; Bollinger, T. K.; Misra, V.; Cryan, P. M.; Blehert, D. S.; Wibbelt, G.; Willis, C. K. R. Pathophysiology of White-Nose Syndrome in Bats: A Mechanistic Model Linking Wing Damage to Mortality. *Biology Letters* **2013**, *9* (4). https://doi.org/10.1098/rsbl.2013.0177.

(13) Lorch, J. M.; Meteyer, C. U.; Behr, M. J.; Boyles, J. G.; Cryan, P. M.; Hicks, A. C.; Ballmann, A. E.; Coleman, J. T. H.; Redell, D. N.; Reeder, D. M.; et al.

Experimental Infection of Bats with *Geomyces destructans* Causes White-Nose Syndrome. *Nature* **2011**, *480* (7377), 376–378. https://doi.org/10.1038/nature10590.

(14) Minnis, A. M.; Lindner, D. L. Phylogenetic Evaluation of *Geomyces* and Allies Reveals No Close Relatives of *Pseudogymnoascus destructans*, Comb. Nov., in Bat Hibernacula of Eastern North America. *Fungal Biology* **2013**, *117* (9), 638–649. https://doi.org/10.1016/j.funbio.2013.07.001.

(15) Rachowicz, L. J.; Hero, J.-M.; Alford, R. A.; Taylor, J. W.; Morgan, J. A. T.; Vredenburg, V. T.; Collins, J. P.; Briggs, C. J. The Novel and Endemic Pathogen Hypotheses: Competing Explanations for the Origin of Emerging Infectious Diseases of Wildlife. *Conservation Biology* **2005**, *19* (5), 1441–1448. https://doi.org/10.1111/j.1523-1739.2005.00255.x.

(16) Warnecke, L.; Turner, J. M.; Bollinger, T. K.; Lorch, J. M.; Misra, V.; Cryan, P. M.; Wibbelt, G.; Blehert, D. S.; Willis, C. K. R. Inoculation of Bats with European *Geomyces destructans* Supports the Novel Pathogen Hypothesis for the Origin of White-Nose Syndrome. *Proceedings of the National Academy of Sciences* **2012**, *109* (18), 6999–7003. https://doi.org/10.1073/pnas.1200374109.

(17) Ren, P.; Haman, K. H.; Last, L. A.; Rajkumar, S. S.; Keel, M. K.; Chaturvedi, V. Clonal Spread of *Geomyces destructans* among Bats, Midwestern and Southern United States. *Emerging Infectious Diseases* **2012**, *18* (5), 883–885. https://doi.org/10.3201/eid1805.111711.

(18) Rajkumar, S. Clonal Genotype of *Geomyces destructans* among Bats with White Nose Syndrome, New York, USA. *Emerging Infectious Diseases* **2011**, *17* (7), 1273–1276. https://doi.org/10.3201/eid1707.102056.

(19) Puechmaille, S. J.; Wibbelt, G.; Korn, V.; Fuller, H.; Forget, F.; Mühldorfer, K.; Kurth, A.; Bogdanowicz, W.; Borel, C.; Bosch, T.; et al. Pan-European Distribution of White-Nose Syndrome Fungus (*Geomyces destructans*) Not Associated with Mass Mortality. *PLoS ONE* **2011**, *6* (4), e19167. https://doi.org/10.1371/journal.pone.0019167.

(20) Puechmaille, S. J.; Verdeyroux, P.; Fuller, H.; Gouilh, M. A.; Bekaert, M.; Teeling, E. C. White-Nose Syndrome Fungus (*Geomyces destructans*) in Bat, France. *Emerging Infectious Diseases* **2010**, *16* (2), 290–293. https://doi.org/10.3201/eid1602.091391.

(21) Wibbelt, G.; Kurth, A.; Hellmann, D.; Weishaar, M.; Barlow, A.; Veith, M.; Prüger, J.; Görföl, T.; Grosche, L.; Bontadina, F.; et al. White-Nose Syndrome Fungus (*Geomyces destructans*) in Bats, Europe. *Emerging Infectious Diseases* **2010**, *16* (8), 1237–1243. https://doi.org/10.3201/eid1608.100002.

(22) Martínková, N.; Bačkor, P.; Bartonička, T.; Blažková, P.; Červený, J.; Falteisek, L.; Gaisler, J.; Hanzal, V.; Horáček, D.; Hubálek, Z.; et al. Increasing Incidence of *Geomyces destructans* Fungus in Bats from the Czech Republic and Slovakia. *PLoS ONE* **2010**, *5* (11), e13853. https://doi.org/10.1371/journal.pone.0013853.

(23) Palmer, J. M.; Kubatova, A.; Novakova, A.; Minnis, A. M.; Kolarik, M.; Lindner, D. L. Molecular Characterization of a Heterothallic Mating System in *Pseudogymnoascus destructans*, the Fungus Causing White-Nose Syndrome of Bats. *G3; Genes|Genomes|Genetics* **2014**, *4* (9), 1755–1763. https://doi.org/10.1534/g3.114.012641.

(24) Zukal, J.; Bandouchova, H.; Brichta, J.; Cmokova, A.; Jaron, K. S.; Kolarik, M.; Kovacova, V.; Kubátová, A.; Nováková, A.; Orlov, O.; et al. White-Nose Syndrome without Borders: *Pseudogymnoascus destructans* Infection Tolerated in Europe and Palearctic Asia but Not in North America. *Scientific Reports* **2016**, *6* (1). https://doi.org/10.1038/srep19829.
(25) Leopardi, S.; Blake, D.; Puechmaille, S. J. White-Nose Syndrome Fungus Introduced from Europe to North America. *Current Biology* **2015**, *25* (6), R217–R219. https://doi.org/10.1016/j.cub.2015.01.047.
(26) Drees, K. P.; Lorch, J. M.; Puechmaille, S. J.; Parise, K. L.; Wibbelt, G.; Hoyt, J. R.; Sun, K.; Jargalsaikhan, A.; Dalannast, M.; Palmer, J. M.; et al. Phylogenetics of a Fungal Invasion: Origins and Widespread Dispersal of White-Nose Syndrome. *mBio* **2017**, *8* (6). https://doi.org/10.1128/mBio.01941-17.
(27) Moore, M. S.; Reichard, J. D.; Murtha, T. D.; Nabhan, M. L.; Pian, R. E.; Ferreira, J. S.; Kunz, T. H. Hibernating Little Brown Myotis (*Myotis lucifugus*) Show Variable Immunological Responses to White-Nose Syndrome. *PLoS ONE* **2013**, *8* (3), e58976. https://doi.org/10.1371/journal.pone.0058976.
(28) Johnson, J. S.; Reeder, D. M.; Lilley, T. M.; Czirják, G. Á.; Voigt, C. C.; McMichael, J. W.; Meierhofer, M. B.; Seery, C. W.; Lumadue, S. S.; Altmann, A. J.; et al. Antibodies to *Pseudogymnoascus destructans* Are Not Sufficient for Protection against White-Nose Syndrome. *Ecology and Evolution* **2015**, *5* (11), 2203–2214. https://doi.org/10.1002/ece3.1502.
(29) Lilley, T. M.; Prokkola, J. M.; Johnson, J. S.; Rogers, E. J.; Gronsky, S.; Kurta, A.; Reeder, D. M.; Field, K. A. Immune Responses in Hibernating Little Brown Myotis (*Myotis lucifugus*) with White-Nose Syndrome. *Proceedings of the Royal Society B: Biological Sciences* **2017**, *284* (1848), 20162232. https://doi.org/10.1098/rspb.2016.2232.
(30) Meteyer, C. U.; Barber, D.; Mandl, J. N. Pathology in Euthermic Bats with White Nose Syndrome Suggests a Natural Manifestation of Immune Reconstitution Inflammatory Syndrome. *Virulence* **2012**, *3* (7), 583–588. https://doi.org/10.4161/viru.22330.
(31) Rapin, N.; Johns, K.; Martin, L.; Warnecke, L.; Turner, J. M.; Bollinger, T. K.; Willis, C. K. R.; Voyles, J.; Misra, V. Activation of Innate Immune-Response Genes in Little Brown Bats (*Myotis lucifugus*) Infected with the Fungus *Pseudogymnoascus destructans*. *PLoS ONE* **2014**, *9* (11), e112285. https://doi.org/10.1371/journal.pone.0112285.
(32) Field, K. A.; Johnson, J. S.; Lilley, T. M.; Reeder, S. M.; Rogers, E. J.; Behr, M. J.; Reeder, D. M. The White-Nose Syndrome Transcriptome: Activation of Anti-Fungal Host Responses in Wing Tissue of Hibernating Little Brown Myotis. *PLOS Pathogens* **2015**, *11* (10), e1005168. https://doi.org/10.1371/journal.ppat.1005168.
(33) Cornelison, C. T.; Keel, M. K.; Gabriel, K. T.; Barlament, C. K.; Tucker, T. A.; Pierce, G. E.; Crow, S. A. A Preliminary Report on the Contact-Independent Antagonism of *Pseudogymnoascus destructans* by *Rhodococcus rhodochrous* strain DAP96253. *BMC Microbiology* **2014**, *14* (1). https://doi.org/10.1186/s12866-014-0246-y.
(34) Hoyt, J. R.; Cheng, T. L.; Langwig, K. E.; Hee, M. M.; Frick, W. F.; Kilpatrick, A. M. Bacteria Isolated from Bats Inhibit the Growth of *Pseudogymnoascus*

destructans, the Causative Agent of White-Nose Syndrome. *PLOS ONE* **2015**, *10* (4), e0121329. https://doi.org/10.1371/journal.pone.0121329.
(35) Zhang, T.; Chaturvedi, V.; Chaturvedi, S. Novel Trichoderma Polysporum Strain for the Biocontrol of *Pseudogymnoascus destructans,* the Fungal Etiologic Agent of Bat White Nose Syndrome. *PLOS ONE* **2015**, *10* (10), e0141316. https://doi.org/10.1371/journal.pone.0141316.
(36) Horrocks, N. P. C.; Matson, K. D.; Tieleman, B. I. Pathogen Pressure Puts Immune Defense into Perspective. *Integrative and Comparative Biology* **2011**, *51* (4), 563–576. https://doi.org/10.1093/icb/icr011.
(37) Cornelison, C. T.; Gabriel, K. T.; Barlament, C.; Crow, S. A. Inhibition of *Pseudogymnoascus destructans* Growth from Conidia and Mycelial Extension by Bacterially Produced Volatile Organic Compounds. *Mycopathologia* **2014**, *177* (1–2), 1–10. https://doi.org/10.1007/s11046-013-9716-2.
(38) Cheng, T. L.; Mayberry, H.; McGuire, L. P.; Hoyt, J. R.; Langwig, K. E.; Nguyen, H.; Parise, K. L.; Foster, J. T.; Willis, C. K. R.; Kilpatrick, A. M.; et al. Efficacy of a Probiotic Bacterium to Treat Bats Affected by the Disease White-Nose Syndrome. *Journal of Applied Ecology* **2017**, *54* (3), 701–708. https://doi.org/10.1111/1365-2664.12757.
(39) Micalizzi, E. W.; Mack, J. N.; White, G. P.; Avis, T. J.; Smith, M. L. Microbial Inhibitors of the Fungus *Pseudogymnoascus destructans*, the Causal Agent of White-Nose Syndrome in Bats. *PLOS ONE* **2017**, *12* (6), e0179770. https://doi.org/10.1371/journal.pone.0179770.
(40) Schneider, C. A.; Rasband, W. S.; Eliceiri, K. W. NIH Image to ImageJ: 25 Years of Image Analysis. *Nat. Methods* **2012**, *9* (7), 671–675.
(41) Guzmán, C.; Bagga, M.; Kaur, A.; Westermarck, J.; Abankwa, D. ColonyArea: An ImageJ Plugin to Automatically Quantify Colony Formation in Clonogenic Assays. *PLoS ONE* **2014**, *9* (3), e92444. https://doi.org/10.1371/journal.pone.0092444.

7. Appendix A – Extended Tabular Data

Table A1. Faure Lab bat information and initial isolated strain count

Bat ID	Sex	Age	Location	Isolated on YMA	Isolated on R2A	Bat ID	Sex	Age	Location	Isolated on YMA	Isolated on R2A
P58	M	A	Molesworth	5	2	P86	F	A	Molesworth	3	1
P60	M	A	Molesworth	4	3	P87	F	A	Molesworth	3	3
P61	M	A	Molesworth	2	1	P89	F	A	Molesworth	0	0
P62	M	A	Molesworth	3	2	P90	F	A	Molesworth	2	1
P63	M	A	Molesworth	3	5	P91	F	A	Molesworth	3	2
P64	M	A	Molesworth	2	3	P92	F	A	Molesworth	1	3
P65	M	A	Molesworth	3	3	P94	F	A	Molesworth	2	5
P66	F	A	Molesworth	2	2	P95	F	A	Molesworth	3	2
P67	F	A	Molesworth	2	2	W181	M	A	Molesworth	2	5
P68	F	A	Molesworth	3	1	R113	F	J	Captivity	2	3
P69	F	A	Molesworth	2	2	R115	M	J	Captivity	2	2
P70	F	A	Molesworth	2	2	R116	F	J	Captivity	4	1
P71	F	A	Molesworth	2	1	R119	M	J	Captivity	3	2
P72	F	A	Molesworth	2	1	R234	M	J	Captivity	2	1
P73	F	A	Molesworth	2	2	R235	M	J	Captivity	3	2
P75	F	A	Molesworth	2	3	R237	M	J	Captivity	2	3
P79	F	A	Molesworth	0	3	R240	F	J	Captivity	2	3
P80	F	A	Molesworth	2	1	R250	M	J	Captivity	2	2
P81	F	A	Molesworth	1	1	R265	F	J	Captivity	2	2
P85	F	A	Molesworth	2	3	R266	M	J	Captivity	2	2

Table A2. Final strain library and morphology

Strain	Source	Identity	Morphology
F1	Faure Lab	Unknown (Fungus)	White-yellow-green, raised
F2	Faure Lab	Unknown (Fungus)	Colourless-grey, long fibres
F3	Faure Lab	Unknown (Fungus)	Purple-brown, solid, shiny, flat
F4	Faure Lab	Unknown (Bacteria)	Bright yellow, opaque, matte
F5	Faure Lab	Unknown (Bacteria)	Yellow-brown, translucent, waxy
F6	Faure Lab	Unknown (Fungus)	Grey/green, flat
F7	Faure Lab	Unknown (Fungus)	Green, soft, flat
F8	Faure Lab	Unknown (Fungus)	Colourless, long fibres
F9	Faure Lab	Unknown (Fungus)	Green with dark green spheres
F10	Faure Lab	Unknown (Fungus)	Colourless, short fibres, lawn
F11	Faure Lab	Unknown (Fungus)	Colourless with dark green spheres
F12	Faure Lab	Unknown (Fungus)	Grey, flat, lawn
F13	Faure Lab	Unknown (Bacteria)	White, opaque, shiny
F14	Faure Lab	Unknown (Fungus)	Brown, flat, lawn
F15	Faure Lab	Unknown (Bacteria)	White, opaque, matte, flat
F16	Faure Lab	Unknown (Bacteria)	White, translucent, shiny
F17	Faure Lab	Unknown (Fungus)	Green with white edge, flat
F18	Faure Lab	Unknown (Bacteria)	Pale yellow, opaque, matte
F19	Faure Lab	Unknown (Bacteria)	White, opaque, matte
F20	Faure Lab	Unknown (Bacteria)	White, opaque, shiny
F21	Faure Lab	Unknown (Bacteria)	Purple-brown, solid, shiny, flat
F22	Faure Lab	Unknown (Fungus)	Green with white edge, raised
F23	Faure Lab	Unknown (Bacteria)	Bright yellow, opaque, shiny
F24	Faure Lab	Unknown (Fungus)	White-yellow-green, raised lawn
F25	Faure Lab	Unknown (Bacteria)	Dark yellow, opaque, matte
F26	Faure Lab	Unknown (Bacteria)	Colorless, pinform, circular
F27	Faure Lab	Unknown (Bacteria)	Pale yellow, opaque, matte
F28	Faure Lab	Unknown (Bacteria)	Pale yellow, opaque, shiny
F29	Faure Lab	Unknown (Bacteria)	Pale yellow, translucent, pinform
F30	Faure Lab	Unknown (Fungus)	Yellow-green, flat, lawn
F31	Faure Lab	Unknown (Fungus)	White-yellow-green, soft
F32	Faure Lab	Unknown (Bacteria)	Bright pink, opaque, matte
F33	Faure Lab	Unknown (Fungus)	White-yellow-green, flat
F34	Faure Lab	Unknown (Bacteria)	Bright yellow, opaque, matte
F35	Faure Lab	Unknown (Fungus)	Grey/green, flat, lawn

F36	Faure Lab	Unknown (Fungus)	White, raised lawn
F37	Faure Lab	Unknown (Fungus)	Grey, flat, lawn
F38	Faure Lab	Unknown (Fungus)	White-yellow, flat, lawn
F39	Faure Lab	Unknown (Bacteria)	Yellow-brown, translucent, waxy
S1	Smith Lab	*Bacillus sp.* [39]	White, translucent, matte, irregular
S2	Smith Lab	*Trichoderma atroviride*[39]	White-yellow-green, raised lawn
S3	Smith Lab	*Lecanicillium sp.* [39]	White, raised lawn
S4	Smith Lab	*Pantoea ananatis*[39]	Pale yellow, translucent, matte
S5	Smith Lab	*Penicillium sp.* [39]	Green-grey, flat, lawn
S6	Smith Lab	*Pseudomonas sp.*[40]	Off-white, translucent, waxy, matte
S7	Smith Lab	Unknown (Fungus)	Brown/purple, flat, lawn
S8	Smith Lab	*Sphingobium sp.* [39]	White-pink, raised irregular
S9	Smith Lab	*Penicillium canescens*[39]	White-green-blue, raised lawn
S10	Smith Lab	*Paecilomyces inflatus* [39]	White-pink, solid, irregular
S11	Smith Lab	*Trichoderma harzianum* [39]	White-yellow-green, soft
C1	Contaminant	Unknown (Fungus)	Colourless, long fibres
C2	Contaminant	Unknown (Bacteria)	White, opaque, shiny
C3	Contaminant	Unknown (Bacteria)	Bright yellow, opaque, shiny
C4	Contaminant	Unknown (Bacteria)	White, translucent, matte
C5	Contaminant	Unknown (Bacteria)	Yellow-brown, translucent, waxy
C6	Contaminant	Unknown (Bacteria)	White, opaque, matte, irregular
Pb	ATCC (28807)	*Pseudogymnoascus bhatti*	Yellow-brown, raised, solid
Pd	Smith Lab	*Pseudogymnoascus destructans*[39]	White-grey, circular, raised
Pp	Smith Lab	*Pseudogymnoascus pannorum*[39]	White-grey, flat, lawn
Pr	Smith Lab	*Pseudogymnoascus roseus*[39]	White-pink, flat, lawn

Table A3. Retention times and relative intensities of induced peaks from UV chromatograms

Pairwise Strains	Retention Time (min)	Relative Intensity (%)
F1x*Pb*	14.5	100
F1x*Pb*	16.5	11.8
F1x*Pb*	18.0	89.0
F1x*Pd*	3.7	22.2
F1x*Pd*	10.1	12.8
F1x*Pd*	13.5	26.5

F1x*Pp*	11.9	5.8
F1x*Pp*	12.2	17.9
F1x*Pp*	13.5	16.4
F1x*Pp*	14.5	75.8
F1x*Pp*	16.5	10.6
F1x*Pp*	18.0	100
F1x*Pr*	26.0	7.5
F1x*Pr*	26.5	12.8
F3x*Pd*	10.5	11.8
F3x*Pr*	26.0	14.3
F3x*Pr*	26.6	11.6
S2x*Pb*	8.3	14.3
S2x*Pb*	11.4	4.9
S2x*Pd*	7.5	7.0
S2x*Pd*	24.3	10.6
S8x*Pr*	26.1	13.9
S8x*Pr*	26.6	10.3

Table A4. Retention times, relative intensities, and associated masses of compounds from total ion chromatogram of crude S9 extract

Retention Time (min)	Relative Intensity (%)	Mass List (m/z) *
3.1	7.0	206.0, 234.0, 247.0 262.0, **469.0**
5.4	26.5	206.0, 234.0, **261.0**, 278.0, 289.0
6.0	7.7	216.0, 263.0, 370.0, 422.0, **454.0**
9.2	8.3	168.0, **185.1**, 213.0, 256.0, 526.1
9.7	47.9	168.1, **185.1**, 213.0, 256.0, 508.1
10.5	33.5	165.0, 199.9, **214.9**, 224.0, 375.0
10.9	19.4	156.1, 182.0, 185.0, **197.0**, 278.0
11.6	38.8	168.0, **185.1**, 213.0, 258.1, 510.1
12.1	32.9	148.0, 202.0, 265.1, **584.2**, 606.2
15.5	35.5	441.0, 438.0, 611.0, 629.1, **1235.1**
17.7	100	185.1, **197.1**, 213.1, 225.1, 569.1

*Base peak for each compound is bolded

8. Appendix B – Spectral Data

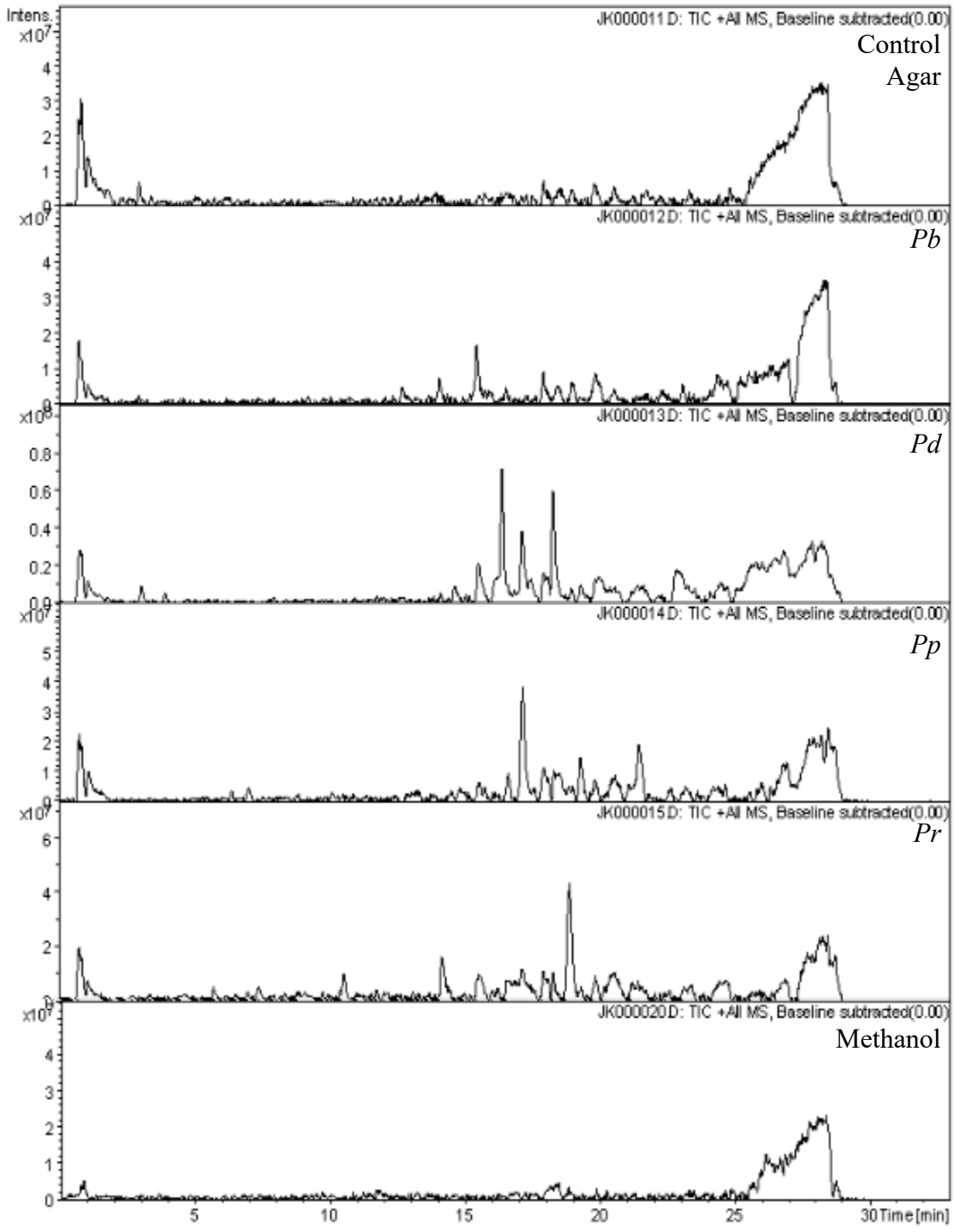

Figure B1. Total ion chromatograms of *P*-strain extracts and controls

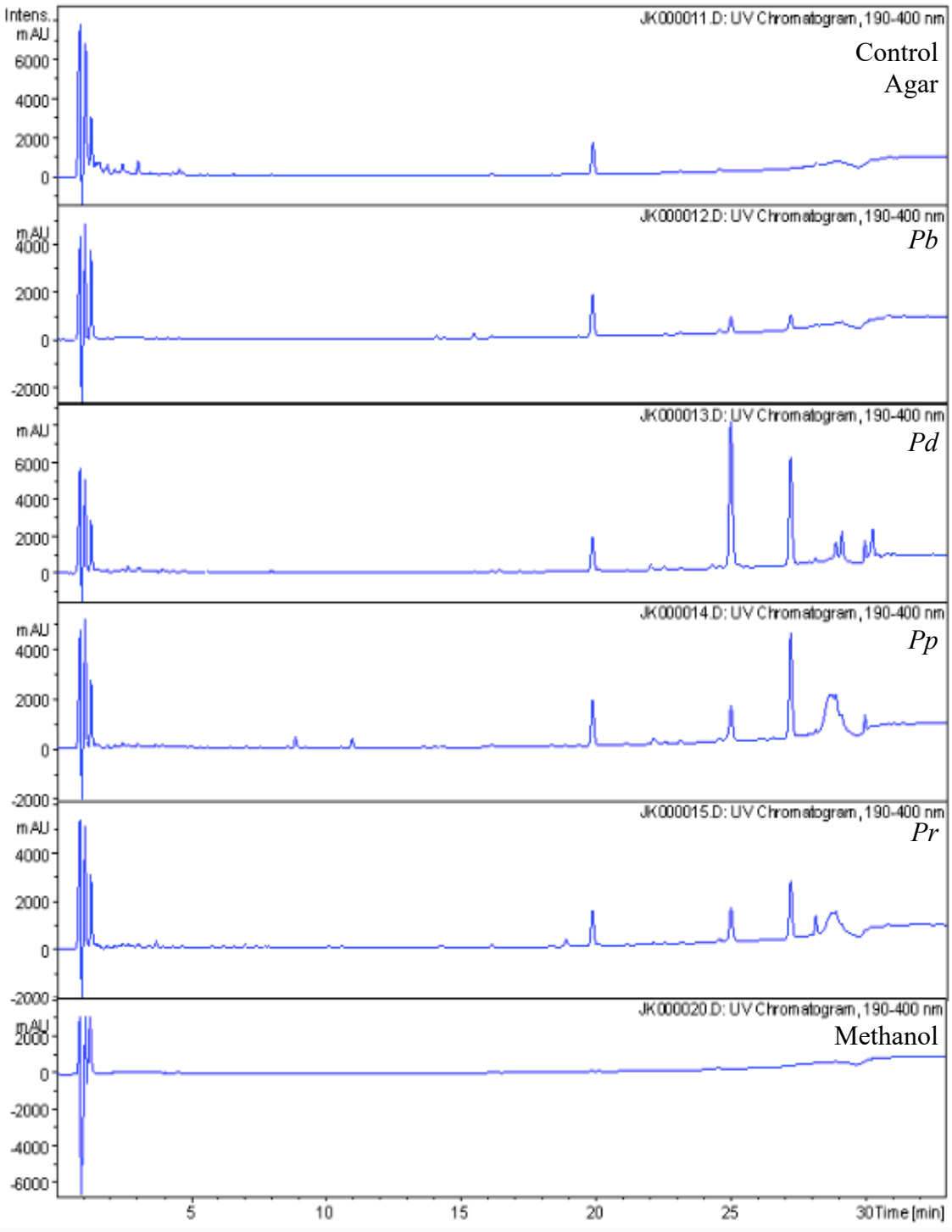

Figure B2. Full range UV chromatograms of *P*-strain extracts and controls

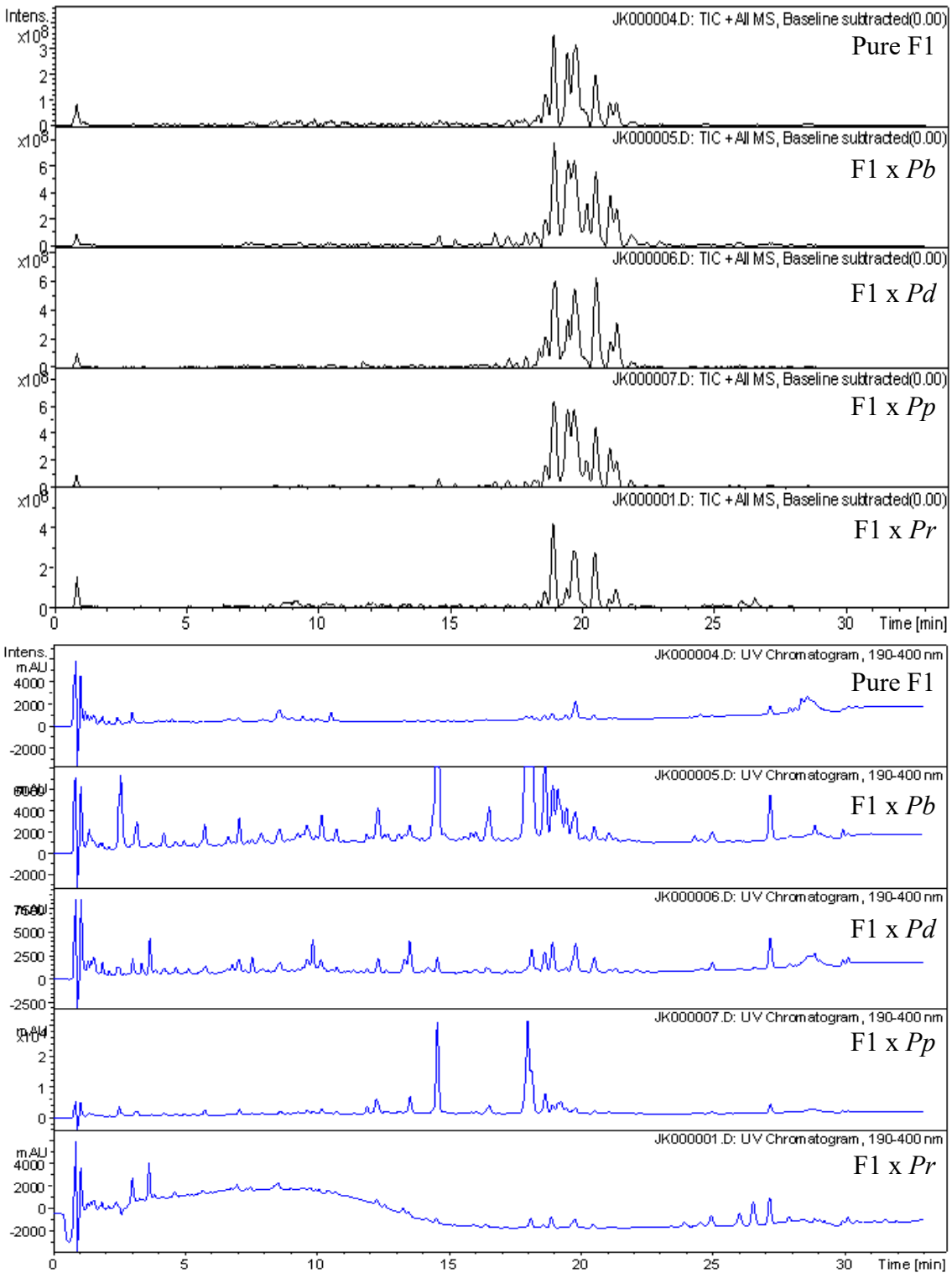

Figure B3. Total ion chromatograms (black) and full range UV chromatograms (blue) of F1 pure and pairwise extracts

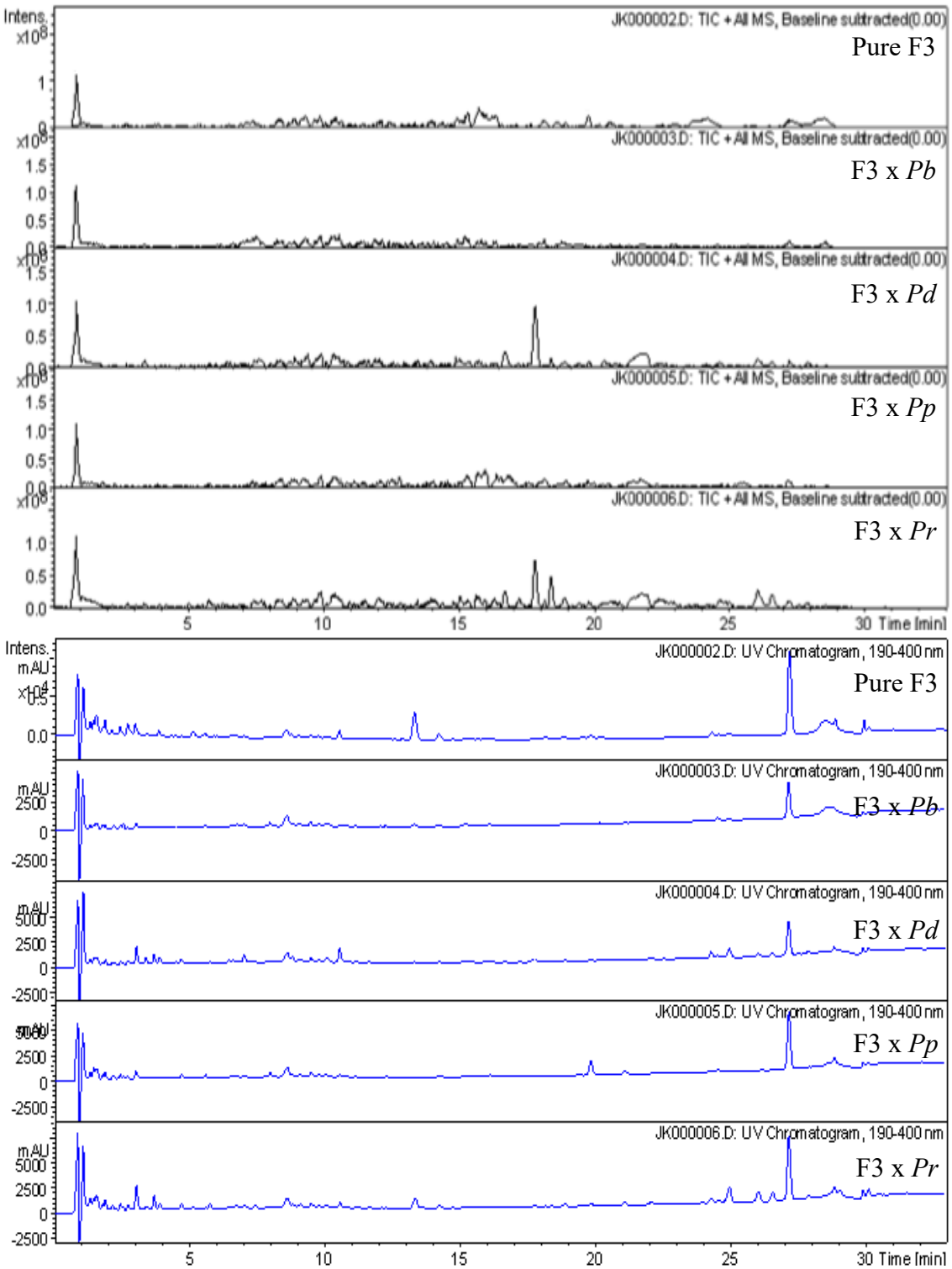

Figure B4. Total ion chromatograms (black) and full range UV chromatograms (blue) of F3 pure and pairwise extracts

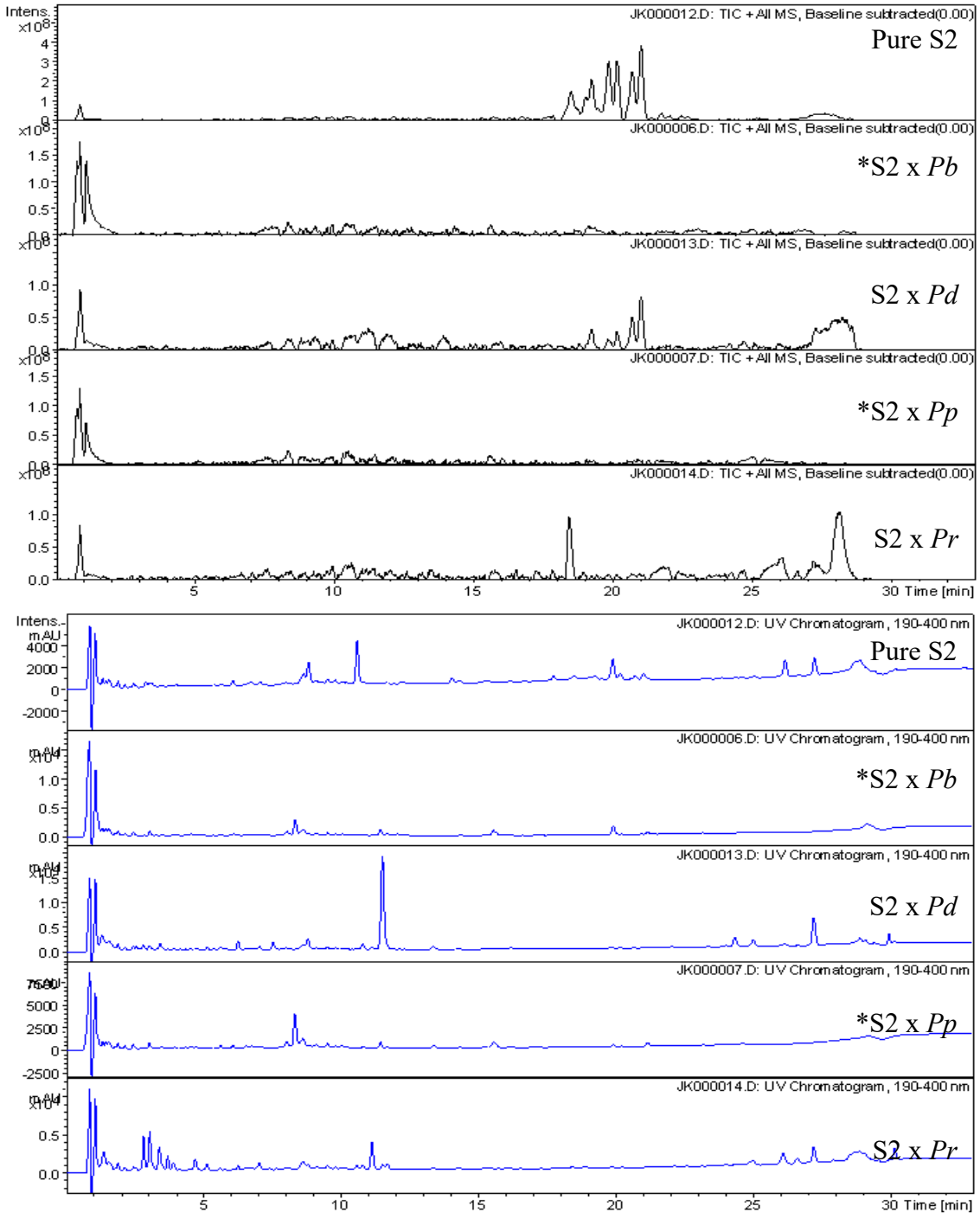

Figure B5. Total ion chromatograms (black) and full range UV chromatograms (blue) of S2 pure and pairwise extracts

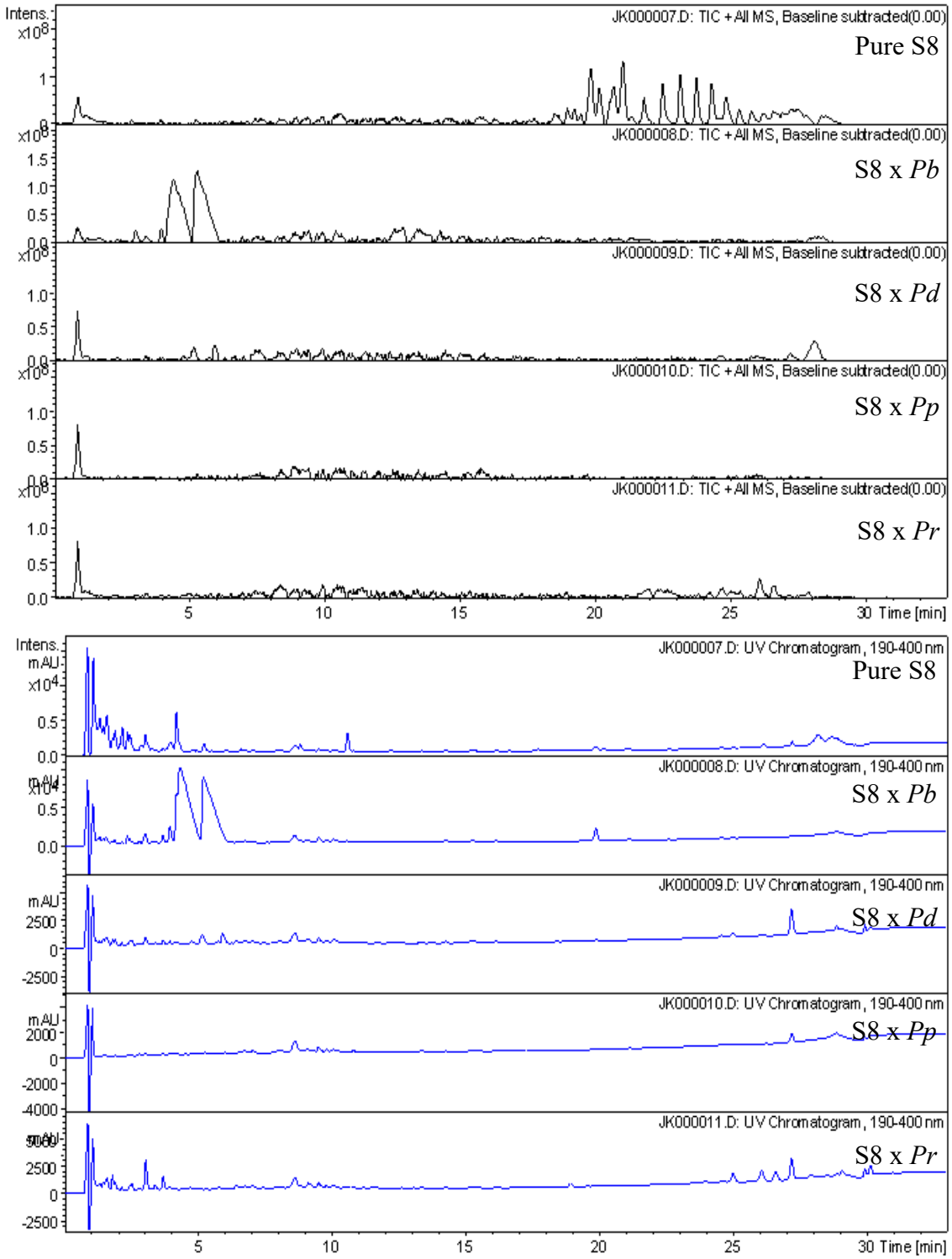

Figure B6. Total ion chromatograms (black) and full range UV chromatograms (blue) of S8 pure and pairwise extracts

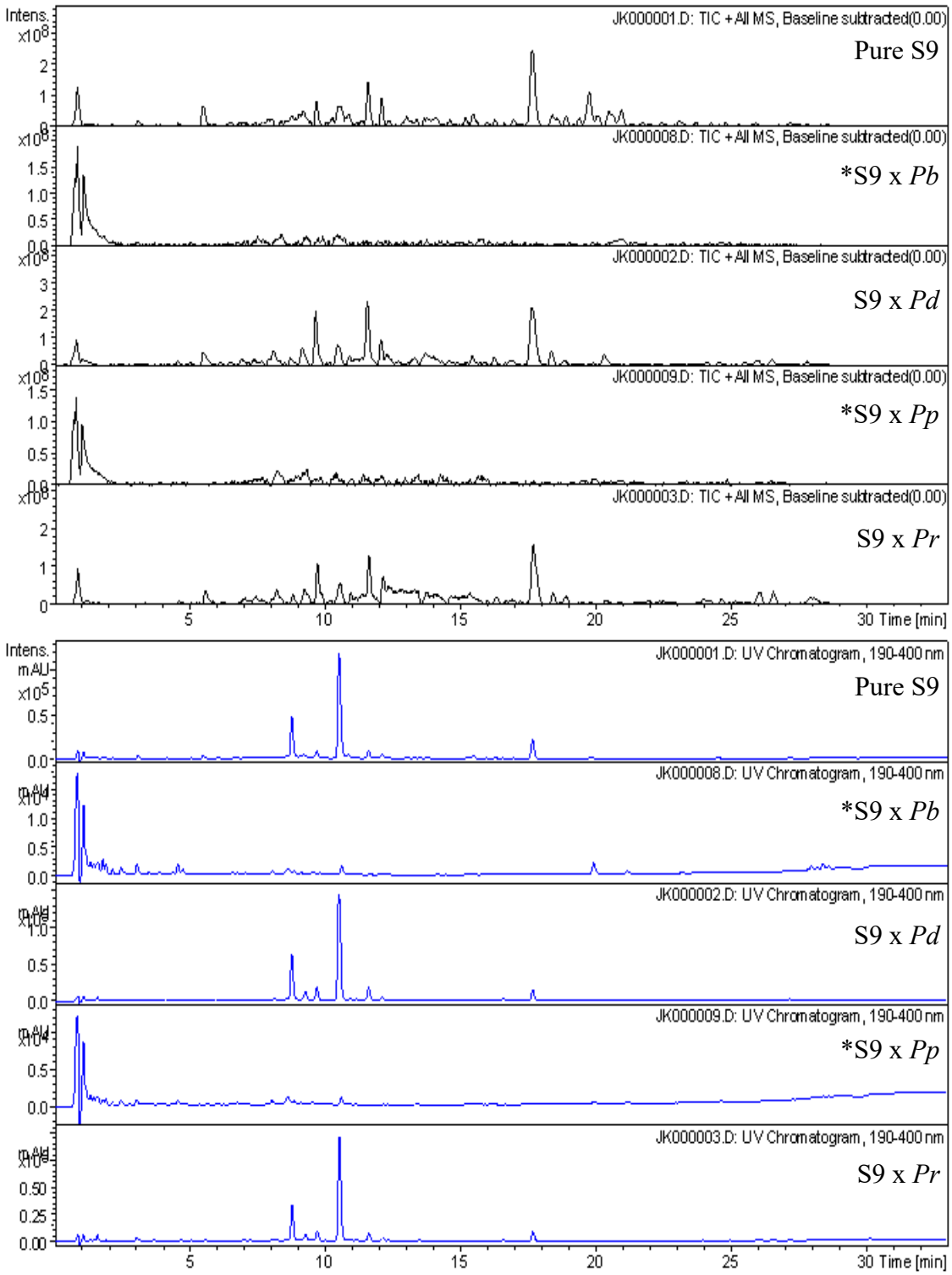

Figure B7. Total ion chromatograms (black) and full range UV chromatograms (blue) of S9 pure and pairwise extracts

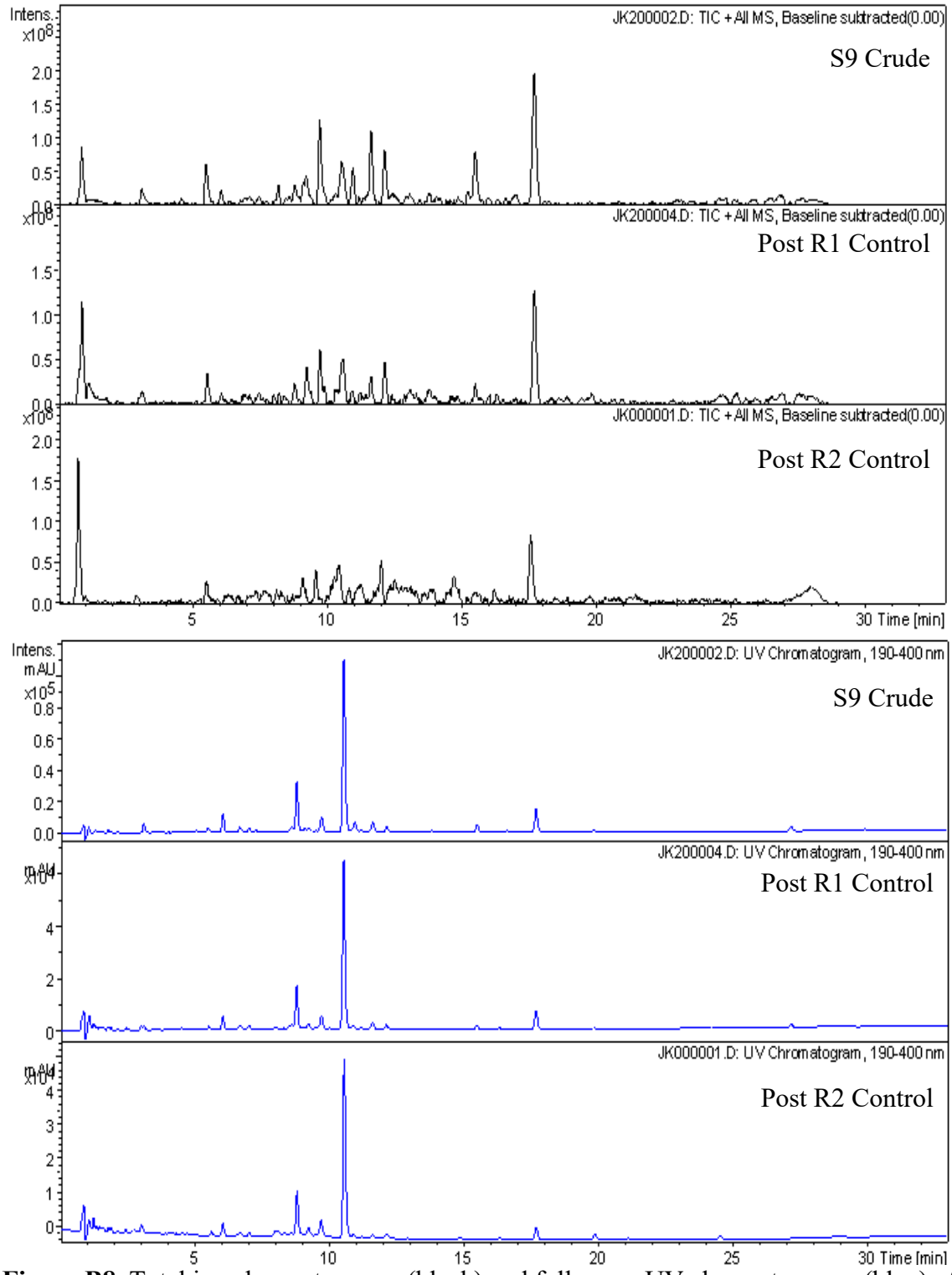

Figure B8. Total ion chromatograms (black) and full range UV chromatograms (blue) of S9 supplemented media controls.

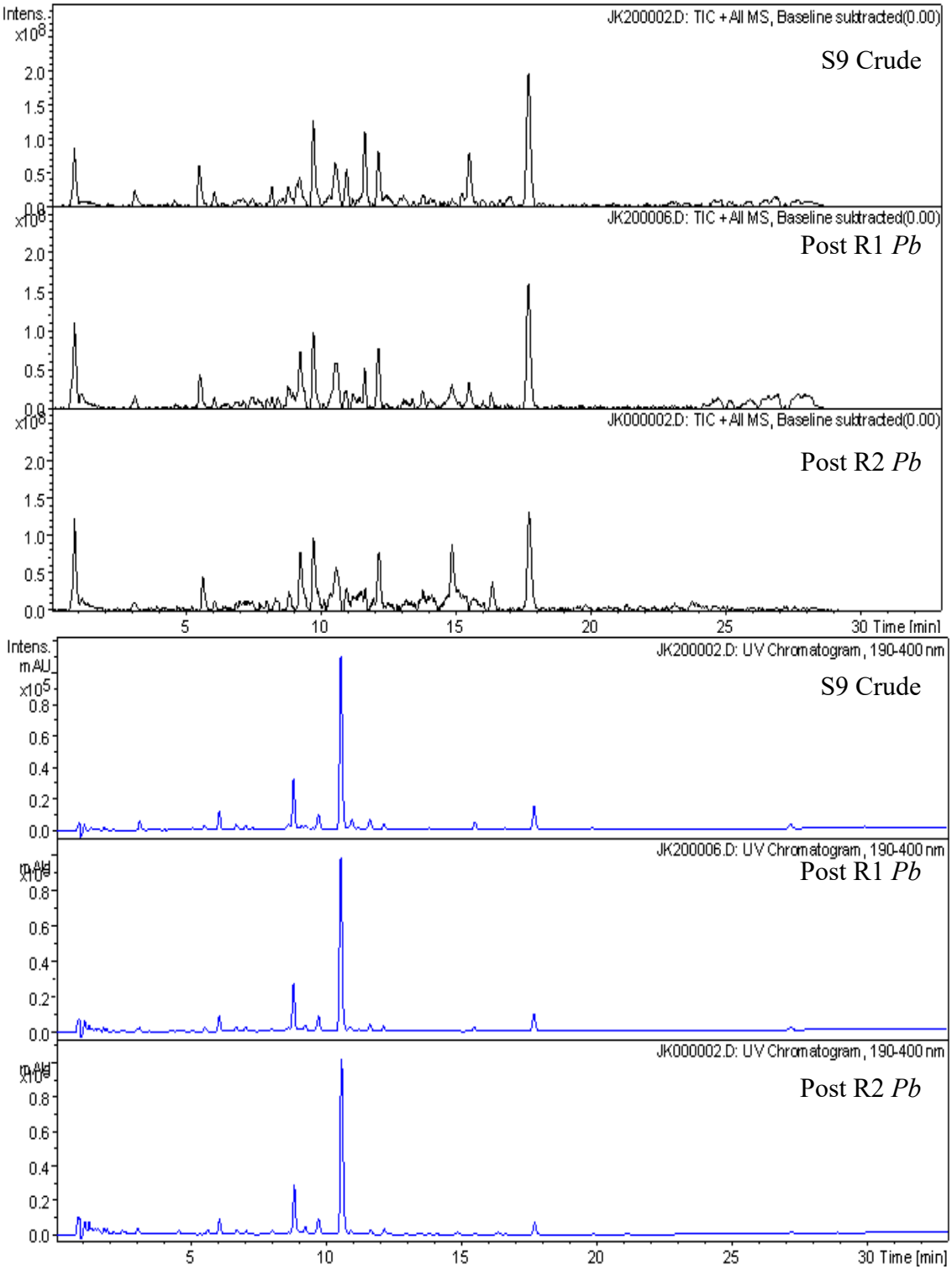

Figure B9. Total ion chromatograms (black) and full range UV chromatograms (blue) of *Pb* on S9 supplemented media

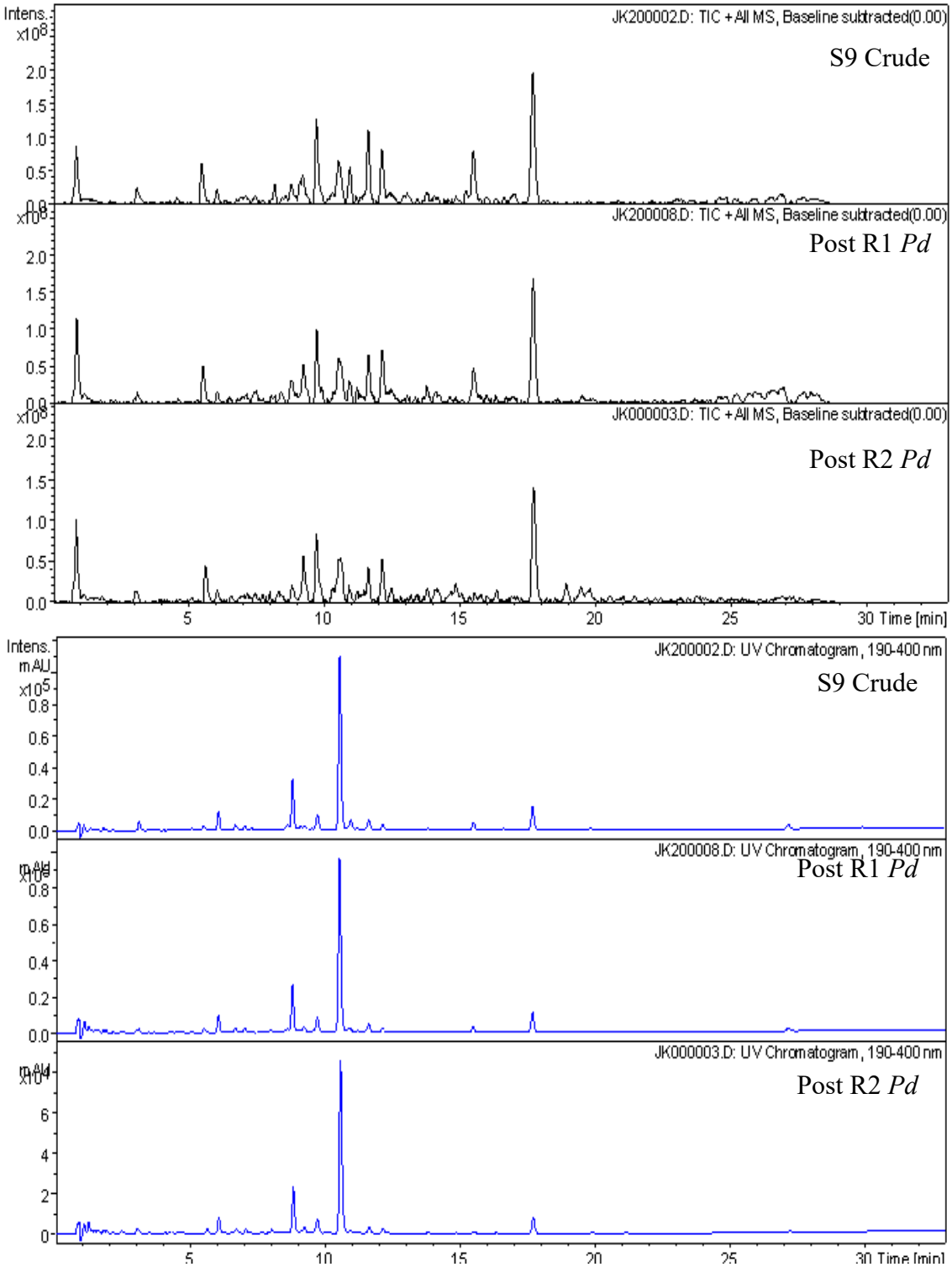

Figure B10. Total ion chromatograms (black) and full range UV chromatograms (blue) of *Pd* on S9 supplemented media

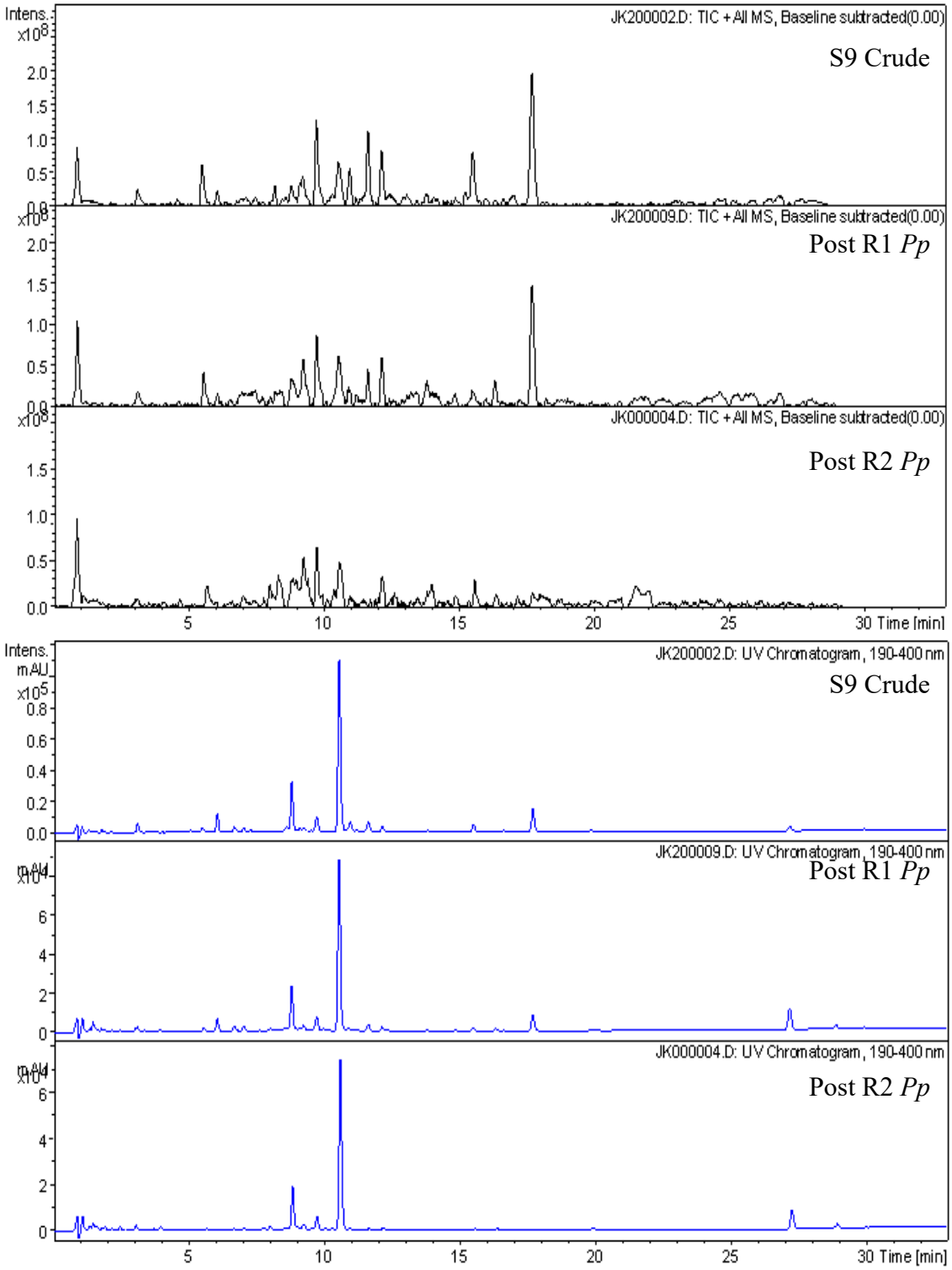

Figure B11. Total ion chromatograms (black) and full range UV chromatograms (blue) of *Pp* on S9 supplemented media

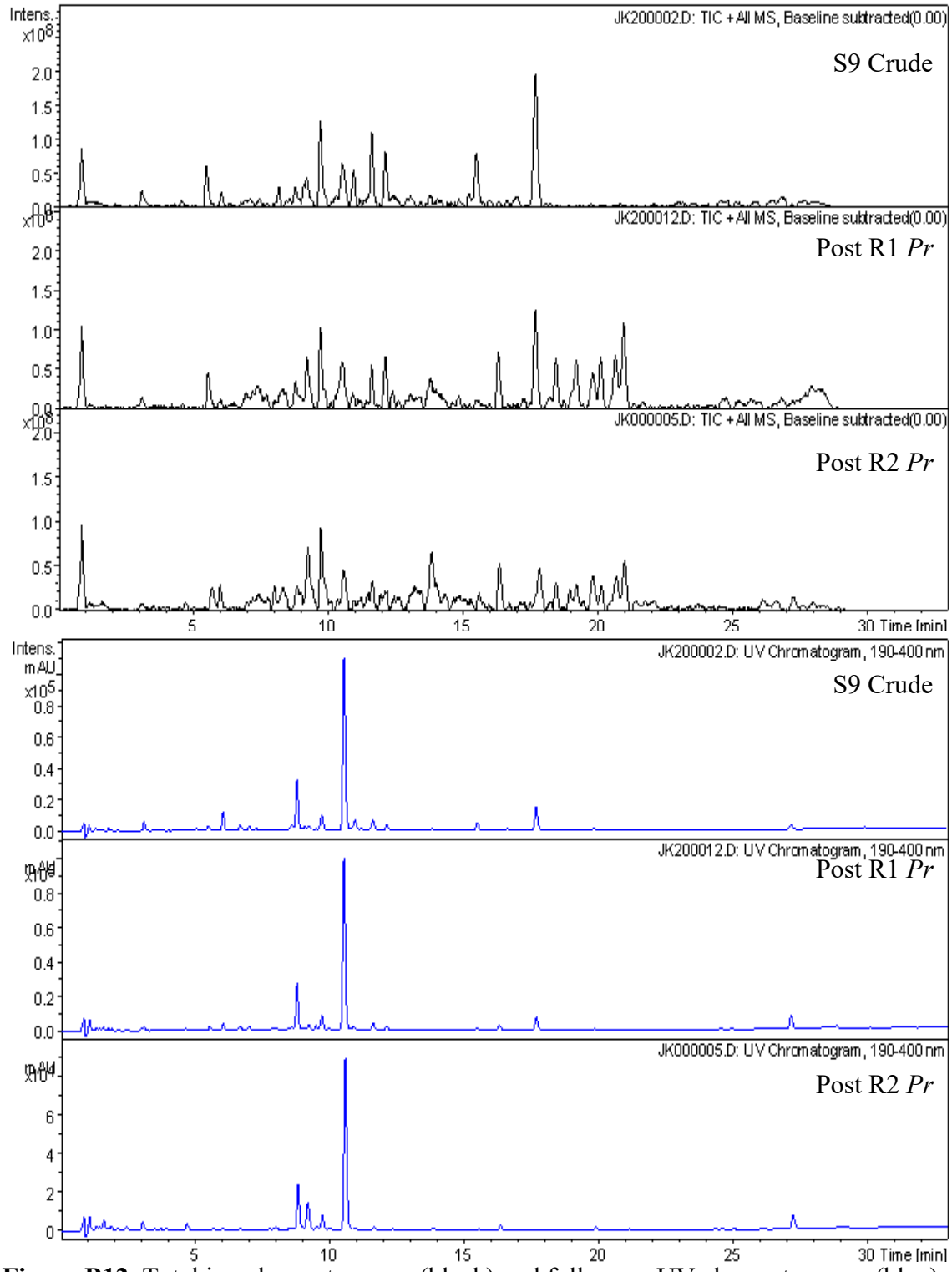

Figure B12. Total ion chromatograms (black) and full range UV chromatograms (blue) of *Pr* on S9 supplemented media